Journal of Hazardous Materials 514 (2026) 142667

Contents lists available at ScienceDirect

Journal of Hazardous Materials

journal homepage: www.elsevier.com/locate/jhazmat

Nanoplastics perturb extracellular vesicle-mediated communication in the *in vitro* and *ex vivo* bone marrow microenvironment of multiple myeloma

Alessandro Villa [a,1], Valentina Citro [a,1], Giulia Sauro [a], Paolo Ciana [a], Raffaella Chiaramonte [a,2], Domenica Giannandrea [a], Natalia Platonova [a], Elena Lesma [a], Clara Bernardelli [a], Beatrice De Felice [b], Mauro Turrini [c], Francesca Guidotti [c], Martina Chiu [d], Marco Parolini [b,1,2], Lavinia Casati [a,*,1,2]

[a] *Department of Health Sciences, University of Milan, Via A di Rudinì 8, Milan 20142, Italy*
[b] *Department of Environmental Science and Policy, University of Milan, via Celoria 26, Milan I-20133, Italy*
[c] *Division of Hematology, Valduce Hospital, Via Dante Alighieri, 11, Como 22100, Italy*
[d] *Department of Medicine and Surgery, University of Parma, via Gramsci 14, Parma 43126, Italy*

HIGHLIGHTS

- Nanoplastics (NPs) induce perturbations of the in vitro bone marrow (BM) microenvironment.
- NPs drive the alterations in extracellular vesicles (EVs) biogenesis and NP incorporation.
- NP exposure affects EV cargo and the education of the in vitro BM microenvironment.
- NPs acquire biological features, modifying EV-mediated communication.

GRAPHICAL ABSTRACT

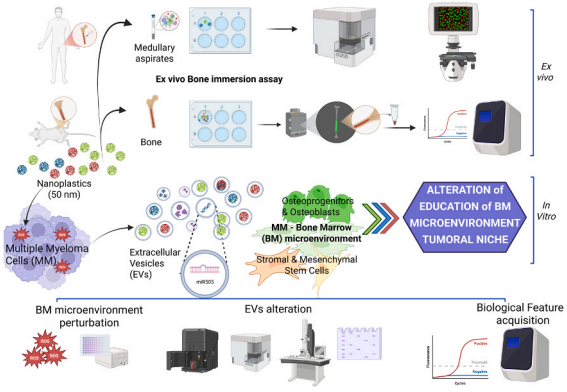

ARTICLE INFO

Keywords:
Nanoplastics
Extracellular vesicles
Bone marrow microenvironment
Oxidative stress
Multiple myeloma

ABSTRACT

Nanoplastics (NPs) are emerging environmental contaminants capable of interacting with biological systems, yet their effects on intercellular communication in the bone marrow (BM) microenvironment remain unclear. This study investigated the impact of polystyrene NPs on extracellular vesicle (EV) biogenesis, cargo, and function using in vitro models of multiple myeloma (MM) and stromal cells, supported by ex vivo murine bone and human BM aspirates. Under the experimental conditions used in this study, NPs were efficiently internalized by both malignant and stromal cells, inducing oxidative stress and reducing cell viability. NP exposure altered EV biogenesis, leading to increased vesicle release, reduced size, and the incorporation of NPs into a subset of EVs. Additionally, EVs from NP-exposed MM cells showed decreased total miRNA content and modulation of miRNA

* Corresponding author.
E-mail address: lavinia.casati@unimi.it (L. Casati).
[1] These authors contribute equally
[2] CRC Nano/microplastics on Environments, Medicine, Ecology, Systems Interaction Studies – NEMESIS, University of Milan

https://doi.org/10.1016/j.jhazmat.2026.142667
Received 7 January 2026; Received in revised form 8 June 2026; Accepted 8 June 2026
Available online 9 June 2026

sorting-related proteins. Among the analyzed miRNAs, miR-505, a candidate linked to osteogenic regulation, was reduced in both cells and EVs following NP exposure. Functionally, EVs from control MM cells downregulated osteogenic markers in pre-osteoblasts, whereas EVs from NP-exposed cells showed reduced regulatory effects. These findings demonstrate that NP exposure modifies EV-mediated signaling under experimental conditions, providing mechanistic insight into nanoplastic interference with BM cellular communication.

1. Introduction

1.1. Nanoplastic: one health issue?

Over the past decade, plastic pollution has become one of society's most widely acknowledged environmental and public health challenges. The rise in plastic production, coupled with poor end-of-life plastic waste management, has led to the accumulation of plastics in the environment. Once released, plastics degrade or fragment through physical, chemical, and biological processes, breaking into smaller micro- and nanoplastics [1,2]. Nanoplastics (NPs), however, are defined as particles from 1 nm $\leq x \leq$ 1 μm [3]. The size ranges of micro- and NPs overlap slightly, and the definition of microplastics should be revisited, with the lower limit set to 1 μm [4]. NPs are released in the environment via various pathways, including the fragmentation of larger plastic objects and the disintegration of synthetic fibers during washing [5,6]. Recent studies have identified NPs in freshwater, marine environments, sediments, and soils [7], highlighting wide distribution in the environment and their potential toxicity in aquatic and terrestrial organisms, affecting the metabolism and energy processes and the oxidative stress balance (OS) [8–12]. Additionally, a recent review has outlined the presence, exposure routes, ecotoxicity, and possible effects of NPs on human health [13], as these particles can enter the human body through inhalation and ingestion. A recent study has observed the presence of NPs in human blood, specifically polyethylene terephthalate (PET), polystyrene (PS), and polyethylene (PE), with an average concentration of 1.6 μg of total plastic particles per milliliter of blood sample [14]. Once inside the human body, NPs can be internalized by cells through mechanisms such as phagocytosis and endocytosis [15]. Recent studies found microplastics and NPs in the human brain [16], placenta [17], macrophage [18], and atherogenic plaques [19]. NPs have also been found to infiltrate the bone marrow (BM), [20−22]. Some *in vitro* and *in vivo* studies suggest that NPs may severely impact the human body, leading to negative effects, including the onset of physical stress, cellular damage, inflammation [23], and immune responses [24]. Moreover, the micro(nano)plastics found in atheroma correlate with increased cardiovascular risk [19].

1.2. NPs: a new source of oxidative stress (OS)?

Research on NPs toxicity has demonstrated that, once inside cells, NPs trigger the overproduction of reactive oxygen species (ROS) and cause OS in aquatic organisms used as ecological indicators [25], murine models [26], and human cell lines [27]. This oxidative dysregulation has been proposed as a key mechanism underlying the adverse outcomes associated with NP exposure [27]. Indeed, ROS are crucial players in disrupting skeletal integrity during aging [28]. Under physiological conditions, ROS disrupt the balance between critical processes of bone remodeling, such as resorption and deposition. Our previous work has shown that NPs negatively impact bone by increasing ROS production [23], suggesting that NPs may interfere with bone cell activities in physiological conditions, thereby affecting bone remodeling and potentially increasing the risk of osteoporotic fractures.

1.3. The bone microenvironment: NPs affect both naive and pathological states

The initial OS-induced disruption of bone [29] alters the behavior of mesenchymal stromal cells (MSCs), driving their differentiation toward adipocytes (ADs) instead of osteoblasts (OBs). This imbalance in differentiation, induced by OS, is a critical process not only under naive conditions but also in pathological states like cancer: the bone acts as a favourable niche for various cancers, including multiple myeloma (MM) [30], a malignancy of transformed plasma cells accumulating in the BM. Bone loss, a hallmark of MM, is promoted by malignant plasma cells [31] and sustains tumor progression [32].

1.4. Extracellular vesicles (EVs): an innovative target for NPs

The bone microenvironment relies on a well-regulated communication network in which extracellular vesicles (EVs) play a vital role [33]. EVs are membranous structures derived from cells, originating from the endosomal system or the plasma membrane [34]. They facilitate intercellular communication, especially within cancer niches like the MM microenvironment, by transferring specific functional molecular cargo, such as proteins and miRNAs [35,36]. Recent studies have highlighted that the biogenesis, lipid composition, and cargo of EVs can be influenced by OS [37]. More recently, EVs have also emerged as biologically relevant targets of nanomaterial-induced perturbation. Nanomaterial exposure can alter EV biogenesis, release, size distribution, and cargo composition, thereby modifying the signaling activity of EVs toward recipient cells. In addition, bidirectional interactions between nanoparticles and EVs have been proposed, including the possibility that nanoparticles may be incorporated into EVs or influence EV-associated trafficking pathways. These observations provide a rationale for investigating EVs as sensitive mediators and targets of nanoplastic-induced cellular stress. [38−40]. A recent paper demonstrated that EVs could serve as an intercellular communication system between bone and BM adipose tissue for transporting osteogenic factors, thus promoting pro-osteogenic processes [41].

1.5. Role of EVs in MM

We recently demonstrated the pivotal role of MM-derived EVs (MM-EVs) in educating the tumoral niche, in particular promoting angiogenesis and osteoclastogenesis [42]. Indeed, MM-EVs are key players in BM microenvironment education and the osteogenic process. Faict and coauthors show that MM-EVs create a supportive bone microenvironment for MM, resulting in the downregulation of *Runx2*, a key master gene of osteoblast differentiation [43].

Given these premises, it holds relevance to explore the impact of NP-induced OS on the bone microenvironment through the crosstalk mediated by MM-derived EVs. Therefore, the present study aims to investigate the effects of NPs on EV-mediated interactions within the *in vitro* MM bone niche, using both stromal and multiple myeloma cells as models.

2. Experimental

2.1. Cell cultures

The murine osteoblastic cell line MC3T3-E1 was purchased from ATCC (cat. CRL−2593) and was seeded in High Glucose Dulbecco's modified Eagle's medium (DMEM; Euroclone, Italy) supplemented with 10% fetal bovine serum (FBS; Euroclone, Italy), 100 U/ml penicillin/streptomycin (Euroclone, Pero, Italy) and 2 mM L-glutamine (Euroclone,

Pero, Italy) as previously reported [44]. We replaced the culture medium twice weekly, and MC3T3-E1 cells were trypsinized weekly and re-plated for continued proliferation.

The human MM cell line OPM2 (ACC−50) was purchased from the DSMZ collection of microorganisms and was cultured in RPMI1640 medium (Euroclone, Pero, Italy) supplemented with 10% FBS (Euroclone, Pero, Italy), 100 U/ml penicillin/streptomycin (Euroclone, Pero, Italy), and 2 mM L-glutamine (Euroclone, Pero, Italy).

Human stromal cells HS5 were purchased from ATCC (cat. CRL−3611) and were seeded in High Glucose DMEM (Euroclone, Pero, Italy) supplemented with 10% FBS (Euroclone, Pero, Italy), 100 U/ml penicillin/streptomycin (Euroclone, Pero, Italy) and 2 mM L-glutamine. We replaced the culture medium twice weekly, and HS5 cells were trypsinized weekly.

2.2. NP treatment

Fluorescent, spherical polystyrene NPs (diameter 50 nm, Excitation/emission peaks of 468/508 nm (Green), 542/612 nm (Red), and 365/447 nm (Blue), aqueous solution 1% solids) were purchased by ThermoFisher Scientific (USA). NPs were used following the manufacturer's instructions. The treatments ranged from 1 μg/ml to 200 μg/ml, and the cell exposure time was from 4 to 96 h, depending on the experimental plan. NPs were used to treat MC3T3-E1, OPM2, and HS5 cells. For uptake experiments, green NPs were used at 1–200 μg/ml for 48 h. For cell viability, green NPs were used at 1–200 μg/ml for 48 h. For ROS production, red NPs were used at 1–200 μg/ml for 48 h. For the transcriptomic analysis, green NPs were used at 100 μg/ml for 48 h. For the ex vivo experiments on excised murine bone, red NP were used at 200 μg/ml for 24 h. The NP concentrations used in this study were intentionally selected to induce robust and reproducible mechanistic responses under controlled conditions and do not aim to reproduce physiological exposure levels (see our previous paper [23]). In particular, the 200 μg/ml condition used in the ex vivo bone immersion assay should be regarded as a high-dose mechanistic challenge to test tissue permissiveness, NPs retention, and early molecular responses, rather than as a quantitative surrogate of in vivo exposure within the bone marrow compartment. Indeed, to investigate whether these emerging contaminants are capable of perturbing tumor–microenvironment communication under controlled experimental conditions, the experimental design was intentionally configured to maximize the detection of early molecular and EV-mediated responses to nanoplastic exposure, rather than to reproduce chronic environmental exposure scenarios or realistic tissue burdens.

2.3. Ex vivo experiments

Four female C57BL/6 mice (12 months old) were used to obtain bone samples for *ex vivo* analysis. Animals used for *ex vivo* experiments were maintained under specific pathogen-free (SPF) housing conditions prior to tissue collection. Consequently, the *ex vivo* bone samples represent a controlled experimental system and were not intentionally preconditioned through environmental nanoplastic exposure before tissue collection. All animal procedures were carried out in accordance with the FELASA guidelines and approved by the Italian Ministry of University and Research (permission numbers: 5247B.N.459/2019 and 12–12–30012012/2012). The mice were housed in individually ventilated plastic cages under controlled temperature (22–25 °C) and humidity (50% ± 10%) conditions, with a 12:12 h light/dark cycle (lights on at 07:00). Food and water were provided ad libitum, and cages were enriched with nesting material. After euthanasia by CO_2 inhalation, the femurs and tibiae (with periosteum intact) were aseptically dissected from each animal. The surrounding muscles were gently removed under sterile conditions, and the tip of each bone was cut off using a rongeur. The bone samples were then incubated at 37 °C in α-minimal essential medium (α-MEM; Gibco, Waltham, MA, USA) supplemented with 5% fetal bovine serum (FBS), 5% calf serum, and 1% penicillin–streptomycin. Either vehicle or fluorescent NPs was added to the medium during this 24 h incubation. *Ex vivo* fluorescence imaging was performed immediately after the incubation period using an IVIS Spectrum imaging system (PerkinElmer, Waltham, MA, USA) equipped with appropriate filters to detect the NP fluorescent signal (ex:542 nm/em:612 nm), in accordance with the manufacturer's instructions. Immediately after imaging, bone marrow was harvested by inserting a 27-gauge needle (attached to a syringe) into one end of each bone and flushing with α-minimal essential medium. The resulting cell suspension was collected and centrifuged for 5 min to pellet the cells, and the supernatant was removed. The cell pellet was then lysed by adding 700 μL of Qiazol reagent (Qiagen, Hilden, Germany). The lysate was homogenized using a TissueLyser (Qiagen, Hilden, Germany) for three cycles of 30 s at 30 Hz, and the samples were centrifuged to remove debris. Approximately 700 μL of the resulting supernatant was used for RNA purification using miRNeasy mini kit column following the protocol provided by the manufacturer (Qiagen, Hilden, Germany)

2.4. NP uptake in in vitro and ex vivo models

To analyze NPs uptake by flow cytometry, OPM2 and HS5 cells were seeded (50,000 cells/well) in a 24-well plate. After 24 h, the monolayer was treated with increasing concentrations (1, 10, 100, and 200 μg/ml) of green NPs for 4 h at 37 °C or 4 °C, as described in our previous paper [23]. The incorporation of NPs was evaluated in the FITC channel at the FACS Verse flow cytometry (BD Biosciences, Italy).

To assess NPs uptake by flow cytometry, total bone marrow aspirate from a multiple myeloma patient (protocol code 285/2023 and date of approval 14/06/2023) was passed through a 100-μm cell strainer and briefly centrifuged to remove debris. Cells were then resuspended and seeded at a concentration of 1×10^6/ml in RPMI−1640 medium supplemented with 10% fetal bovine serum (FBS). Samples were either exposed or not exposed to blue NPs for 24 h. After incubation, both suspended and adherent cells were collected, and erythrocytes were lysed using an ammonium chloride lysis buffer. After centrifugation (300 g for 5 min) we resuspended the pellet with 1 ml of PBS (around 2 × 10^7 cells). We took an aliquot of approximately 150 μL of the remaining cells (corresponding to 3 × 10^6 cells). We incubated these cells with FCR blocking solution (1:30, BioLegend, USA) for 10 min at room temperature and then we stained with antibodies specific for CD138 (1:15, CD138 PE, BD,561704, Mouse IgG1, κ), CD45 (1:30, BV510 Mouse IgG1, κ N.563204 BD Biosciences), and CD90 (1:30, CD90-Thy−1- eBio5E10 BV786 Mouse IgG1, κ eBioscience™, Invitrogen 47–0319–42). Cell viability was assessed using a LIVE/DEAD viability dye (1:300 Fixable Near-IR Dead Cell Stain Kit LD APC H7, Thermofisher-Invitrogen, L34975). A minimum of 500000 events per sample was acquired using a Cytek Aurora Flow cytometer (Cytek Biosciences, California, USA).

2.5. Extracellular vesicle isolation

Cells (OPM2 and MC3T3-E1) were seeded at a density of 3 × 10^5 cells/ml in RPMI1640/DMEM without serum. After 24 h, cell debris and aggregates were removed by centrifugation at increasing speeds of 1000 g, 2000 g, and 3,000 g for 15 min at 4 °C, and EVs were collected by 75 min ultracentrifugation at 110,000 g at 4 °C using a Himac CP100NX ultracentrifuge (Himac, Japan). The obtained pellet was resuspended in 0,1 mm filtered PBS to characterize size and concentration by Nanoparticles Tracking Analysis (NTA, Malvern Panalyticals, UK), the morphology by Cryo-Electron Microscopy (Cryo-EM, FEI TALOS ARTICA, Thermofisher Scientific, USA) analysis, and the uptake and the NPs positivity by flow cytometry analysis. For Western Blot analysis, EVs were resuspended in Laemmli buffer (62.5 mM Tris-HCl pH 6.8, 7.5% glycerol, 2% SDS, 0.125 M dithiothreitol) and quantified using a Bradford assay (Himedia, Italy).

2.6. Nanoparticle tracking analysis (NTA)

Size distribution and concentration of EVs exposed or not to NPs were analyzed by NTA using Nanosight model NS300 (Nanosight, Malvern Panalytical, UK) equipped with green (532 nm, 70 mV) laser, high-pass filter, and sCMOS camera. NTA was performed for each sample by recording five 60 s videos, subsequently analyzed using NTA software 3.0 (Nanosight, Malvern). The detection threshold was set to level 5 and camera to level 12, or camera to level 15 for the acquisition of fluorescent signals.

2.7. Extracellular vesicle flow cytometry

EVs from MM cells exposed or not to blue NPs (excitation/emission peaks of 365/447 nm) were stained with CFSE (carboxyfluorescein diacetate succinimidyl ester) (ThermoFisher Scientific, USA) dye diluted in PBS to check their integrity. After 2 h of incubation at 37 °C, the labeled EVs were analyzed at the spectral flow cytometer Cytek AURORA. Events were first analyzed on the B2 (516–533 nm) channel to identify CFSE-positive particles, corresponding to intact EVs. A gate was generated based on CFSE fluorescence to selectively include these positive events. Within this CFSE-positive population, a second analysis was performed on the V4 channel (466–481 nm) to identify events that were also positive for the blue, fluorescent signal corresponding to nanoplastics. This dual-parameter gating strategy allowed for the identification of intact EVs that had internalized the blue nanoplastics. At least 50000 gated events were collected at medium acquisition rate. The acquired particles were plotted against SSC and FSC to determine the percentages of positive events for CFSE/blue NPs.

2.8. Gene expression

We have investigated NPs effects on the osteogenic factor Runx2 in MC3T3-E1 and the OS-responsive enzymes Heme Oxygenase 1 (HO−1) and HSP−60 in OPM2. As previously described, MC3T3-E1 cells (1.5×10^5 cells/well) were plated in 6-well plates and treated with EVs derived from MM cells (wild or exposed to NPs). Adherent cells were harvested, and total RNA was extracted using Purezol according to the manufacturer's instructions (Biorad, USA). OPM2 cells were seeded at a density of 3×10^5 cells/ml in RPMI1640 supplemented with 10% FBS and were treated with 100 μg/ml of NPs. After 48 h of exposure, total RNA was extracted using Purezol according to the manufacturer's instructions (Biorad, USA). RNA pellet concentrations were assessed spectrophotometrically (Absorbance 260 nm, Absorbance 280 nm) using microcuvette G1.0 in Eppendorf Biophotometer (Eppendorf, Italy). Specific sets of primers (see Table 1) were designed according to Casati [45] and synthesized by Eurofins Genomics (Vimodrone, Italy). Specifically we synthesized the following set of primers: for human Heme Oxigenase type 1 (*HO−1)*, Heat Shock Protein 60 (*HSP−60)*, RNA polymerase II (*RNA Pol II*), Heterogeneous nuclear ribonucleoprotein A2/B1 *(HnRNPA2B1)*, Synaptotagmin Binding Cytoplasmic RNA Interacting Protein (*SYNCRIP*), Y-Box Binding Protein 1 (*YBX1*), 18S ribosomal RNA *(18SrRNA)*; for mouse: Runt-related transcription factor 2 (*Runx2)*, Osteocalcin (*OC*) Collagen1a1 (*Col1a1*), Nuclear factor erythroid 2-related factor 2 (*Nrf2),* Heme Oxigenase *1* (*HO1)* and glyceraldehyde−3-phosphate dehydrogenase (*GAPDH*).

Quantitative PCR was performed in OPUS CFX96 (Bio-Rad, Segrate, Italy) using 10 μl of total volume for each well. The efficiency of each set of primers was evaluated in preliminary experiments, and it was found to be close to 100% for the target gene and the housekeeping genes GAPDH, RNA Pol II, and 18S rRNA. According to the manufacturer's protocol, total RNA (1 μg) was retrotranscribed using the iScript Supermix kit (Bio-Rad). The amplification was performed on 10 ng of total cDNA using SYBR chemistry (Promega) according to the manufacturer's protocol. Quantitative PCR was performed according to the following protocol: an initial step of 60 s at 95 °C, followed by 40 cycles of 15 s at 95 °C and 30 s at 60 °C. A dissociation stage with a melting curve analysis was also performed. Five replicates were performed for each experimental point, and the experiment was repeated twice. Gene expression was quantified using the comparative threshold cycle (ΔΔCt) method, considering that the targets and the reference genes have the same amplification efficiency (nearly 100%), verified as first in a standard curve experiment, as previously described [29].

2.9. Western blotting

Cells were collected as shown by Sibilia et al. [29]. Briefly, they were resuspended in Laemmli buffer with the proteases and phosphatases inhibitors cocktail (Sigma Aldrich, Italy), subjected to the Bioruptor (Diagenode, Liège, Belgium) for 5 min (30 s on; 30 s off, high power) prior to heating samples at 95 °C for 5 min. Protein extracts were then centrifuged at 13,200 rpm for 10 min, and supernatants were saved and directly used for immunoblotting. Protein extracts were resolved by 15% polyacrylamide gel electrophoresis in the presence of SDS (15% SDS/PAGE) and transferred to 0.2-μpore nitrocellulose membranes by standard wet procedure. After transfer, membranes were stained with Ponceau S to verify the correct transfer or activated if using TGX Stain Free Gel technologies (Biorad, USA). and then blocked with 5% nonfat milk in TBS-T (20 mM Tris-HCl, pH 7.5, 150 mM NaCl, 0,05% Tween 20) and probed overnight at 4 °C with the primary specific antibodies: anti-H3 (ref. 1791, Abcam, UK, 1:10000), anti-TSG101 (ref. 72312, Cell Signaling, UK, 1:500), anti-CD81 (ref. 52892, Cell Signaling, USA, 1:1000), anti-CD63 (ref. 52090, Cell Signaling, USA, 1:1000) and anti-GAPDH (ref. 9485, Abcam, UK, 1:1000). Membranes were then incubated with the appropriate HRP conjugated species-specific secondary antibodies (Promega, Italy), and electrochemiluminescence was revealed by using ChemiDoc system (BioRad, California, USA). Densitometric analyses were performed using ImageLab (Biorad, California, USA).

Table 1
Set of primers used for gene expression analysis.

Gene	Forward primer (5′–3′)	Reverse primer (5′−3′)	Species
HO−1	CAGCATGCCCCAGGATTTG	AGCTGGATGTTGAGCAGGA	Human
HSP−60	CACCGTAAGCCTTTGGTCATAAT	CTTGACTGCCACAACCTGAAGA	Human
RNA Pol II	GACACAGGACCACTCATGAAGT	GTGCGGCTGCTTCCATAAG	Human
HnRNPA2B1	CAGCAACCTTCTAACTACGGTCC	CACTGCCTCCTGGACCATAGTT	Human
SYNCRIP	TGAGTGGTAAAGTCAAGGTCTGG	GGCAAGGTTGCGTACAAACAGC	Human
YBX1	GCAGGAGAACAAGGTAGACCAG	CTTCATTGCCGTCCTCTCTAGG	Human
18S rRNA	GTAACCCGTTGAACCCCATT	CCATCCAATCGGTAGTAGCG	Human
Runx2	CGAGTCATTTAAGGCTGCAA	AGGCTGTTTGACGCCATAGT	Mouse
OC	AGGAGGGCAATAAGGTAGT	CATAGATGCGTTTGTAGGC	Mouse
Col1a1	GCATGGCCAAGAAGACATCC	CCTCGGGTTTCCACGTCTC	Mouse
Nrf2	TGAAGTTCGCATTTTGATGGC	CTTTGGTCCTGGCATCTCTAC	Mouse
HO1	CACTCTGGAGATGACACCTGAG	GTGTTCCTCTGTCAGCATCACC	Mouse
GAPDH	CATCCCAGAGCTGAACG	CTGGTCCTCAGTGTAGCC	Mouse

2.10. miRNA profiling

miRNA extraction from OPM2 cells and OPM2 EVs was performed with the combination of miRNeasy Mini Kit and RNeasy MinElute Cleanup Kit (Qiagen, USA) following the manufacturer's instructions. The RNA pellet concentrations were assessed spectrophotometrically using microcuvette G1.0 in Eppendorf Biophotometer. Subsequently, the obtained RNA was retrotranscribed (1 μg from cells and 350 ng from EVs) using the TaqMan MicroRNA Reverse Transcription Kit (ThermoFisher Scientific, USA) and Megaplex RT Primers following the manufacturer's instructions. The amplification was performed on 11,205 ng of total cDNA using the TaqMan Universal PCR Master Mix (Thermofisher Scientific, USA) with the CFX96OPUS (Biorad, USA) following the manufacturer's instructions. miRNA−505 expression levels were assessed by quantitative PCR under the following protocol: an initial step of 10 min at 95 °C followed by 40 cycles of 15 s at 95 °C and 60 s at 60 °C. Relative expression quantification was performed by the 2^(-ΔΔCt) method, using U6 or RNU48 as a reference.

2.11. Cryo-EM

Cryo-EM image acquisition was performed at the UNITECH advanced imaging facility (NOLIMITS), established by the Università degli Studi di Milano. Images were acquired using a FEI TALOS ARTICA cryo-electron microscope (Thermofisher Scientific, USA) at magnifications of 45,000 × (0.229 nm/pixel) and 73000 × (0.143 nm/pixel). A total of 150 fields were imaged using the FEI electron microscope equipped with a FEI Falcon 3EC direct electron detector and a Volta phase plate. Prior to imaging, samples were vitrified using a FEI Vitrobot IV system and processed as previously described [46].

2.12. Fluorescence Microscopy

Fluorescence microscopy images were acquired using an EVOS Cell Imaging System (Thermofisher Scientific, USA) microscope at 40 × magnification. Cells derived from bone marrow aspirates were seeded at a density of 2×10^5 cells/ml and exposed to nanoplastics (NPs) at a concentration of 200 μg/ml for 24 h. Images were obtained under the live imaging mode.

2.13. MTT assay

HS5 and OPM2 cellular viability was evaluated using the MTT test, as previously reported [47]. Briefly, cells were seeded at a density of 5000–10,000 cells/well in 96 multiwell plates and incubated at 37 °C with 500 μg/ml 3-(4,5-dimethyl−2-thiazolyl)−2,5-diphenyltetrazoliumbromide (MTT, Sigma-Aldrich Chemical, Italy) for two hours. After the supernatant removal, formazan crystals were suspended in DMSO. The 570 nm absorbance was read at a microplate spectrophotometer (Ensight, Perkin Elmer).

2.14. ROS production

ROS production was measured using 5(6)-carboxy−2′,7-dichlorofluorescin diacetate (CM-DCFA, Sigma-Aldrich, 10 μM), as previously indicated [48]. Briefly, 10000 cells/well were seeded in black 96-well plates and cultured for 24 h. On the day of the experiment, the cells were pre-incubated with NPs for 48 h at increasing concentrations (starting from 1 μg/ml to 200 μg/ml). After adding CM-DCFA, DCF fluorescence was assessed with a spectrofluorophotometer (Ensight, Perkin Elmer) at the excitation (485 nm) and emission (530 nm) wavelength.

2.15. Transfection of MC3T3-E1 cells and EV treatment

MC3T3-E1 pre-osteoblast cells were cultured under standard conditions until reaching approximately 60–70% confluence. Cells were transfected with a miR−505 mimic (30 nM) using Lipofectamine™ RNAiMAX Transfection Reagent (Thermo Fisher Scientific), according to the manufacturer's instructions. Briefly, the miR−505 mimic was diluted in Opti-MEM Reduced Serum Medium and complexed with RNAiMAX reagent. The transfection mixture was added to the cells and incubated for 16 h. Following transfection, a sequential co-treatment was performed by replacing the medium and adding EVs isolated from OPM2 cells previously exposed to NPs. NP-EVs were administered at a concentration corresponding to a 10 × ratio relative to the producing cells and incubated with recipient cells for 48 h. At the end of the treatment, total RNA was extracted, and RUNX2 gene expression was analyzed by quantitative real-time PCR (qPCR).

2.16. Calcification assay

Calcium deposition, an established marker of late osteogenic differentiation, was assessed in MC3T3-E1 cells differentiated for 7 days using Alizarin Red S staining. In brief, cells were seeded in medium supplemented with L-ascorbic acid 50 μg/ml and β-glycerolphosphate (10 mM, both reagents from Merck KGaA (Darmstadt, Germany) (see [29]). Cultures were maintained for 7 days and educated with 10x MM-EV (Control or NPs exposed). After fixation with EtOH, cells were stained with 1 mg/ml Alizarin Red S (pH 5,5) for 1 h. After microscopy observation (OPTIKA Microscopes Italy, contrast phase, objective 4x and 10x), the deposited dye was eluted with 0,6 M HCl and quantified by measuring absorbance at 405 nm.

2.17. In silico analysis

The 3′UTR sequences of human and mouse RUNX2 were analyzed using TargetScan to identify potential binding sites for miR−505. We selected sites with a 7mer-m8 seed match corresponding to the same miR−505 seed sequence conserved between human and mouse. Aligned target sequences were compared across species. For each site, the predicted repression strength (context++ score) and evolutionary conservation (conserved branch length) were recorded. This comparative analysis shows that human miR−505 can bind to and potentially inhibit mouse RUNX2.

2.18. miRNAs array

Total RNA isolated from EVs released by OPM2 cells was analyzed using TaqMan® Low Density Array (TLDA) Human MicroRNA Cards (Applied Biosystem). ΔCt was calculated by normalizing to the endogenous control RNU48. miRNAs with Crt values > 28, AmpScore < 1.24, or missing amplification were considered not reliably amplified and were assigned a Crt value of 29. Experiments have been replicated three times.

2.19. Ethical committee

The Institutional Review Board of Insubria (Italy) approved the design of this study (protocol code 285/2023 and date of approval 14/06/2023). Written informed consent was obtained in accordance with the Helsinki Declaration.

2.20. Statistical analysis

Each experiment was independently replicated 3–6 times. For each experiment, we provided 6 biological replicates. We used GraphPad Prism8 software (GraphPad Software, USA) for all statistical analyses. The results are expressed as the mean ± SEM of at least three independent experiments (6 replicates for each experiment). Differences between groups were evaluated by one-way or two-way ANOVA followed by the Bonferroni post-hoc test or by an unpaired *t*-test.

Significance was set at a p-value lower than 0.05.

3. Results

3.1. NP-induced perturbations of the BM microenvironment

To investigate whether bone is permissive to NP uptake and responsive to NP-induced stress, we first harvested femurs and tibiae from 12-month-old mice, an age corresponding to a middle-aged bone microenvironment, associated with age-related alterations including low-grade inflammation and impaired osteogenic signaling, features relevant to a multiple myeloma-permissive niche [43,49] Bones were incubated *ex vivo* for 24 h with either PBS or red fluorescent polystyrene NPs (50 nm, 200 μg/ml) and subjected to IVIS imaging. As shown in Fig. 1A, NP-treated bones exhibited a pronounced red fluorescence signal compared to controls, indicating substantial NP retention. Quantification of radiant efficiency (Fig. 1B) confirmed a significant increase in fluorescence in NP-exposed samples ($p < 0.01$), demonstrating effective NP uptake by middle-aged bone tissue. To assess molecular responses within the bone marrow compartment, total RNA was purified from flushed marrow and analyzed by quantitative PCR. As shown in Fig. 1C-D-E, expression of Runx2 and its osteogenic targets Osteocalcin *(OC)* and Collagen 1a1 *(Col1a1)* was generally elevated in NP-treated bones, with OC reaching statistical significance ($p < 0.05$). This coordinated pattern is consistent with an acute transcriptional modulation of osteogenic markers in response to NP exposure. Concurrently, increased expression of Nrf2 and its downstream antioxidant gene HO−1 (Fig. 1F-G) indicated the induction of oxidative stress. These findings indicate that middle-aged bone tissue is permissive to NP uptake and responds with coordinated transcriptional changes involving both osteogenic and stress-related pathways. This *ex vivo* model thus provides a mechanistic link between environmental NP exposure and early molecular perturbations in a myeloma-relevant bone niche.

In order to extend the data derived from murine *ex vivo* models to a more clinically relevant disease context, we analyzed the enrichment of NPs in a MM bone marrow microenvironment using medullary aspirate from an MM patient. Specifically, the total cellular content of the aspirate was exposed to NPs for 24 h. We identified $CD90^+$ mesenchymal stromal cells within the viable population, whereas $CD138^+$ MM cells were identified as $CD138^+/CD45^+$ or $CD45^{dim}$ within the viable population from the total medullary aspirate, either exposed or not to fluorescent NPs. As reported in the table, flow cytometry analysis clearly shows that both MM cells ($CD138^+$) and mesenchymal stromal cells ($CD90^+$) are positive for the NP channel at approximately 100% following exposure (Table 2).

These results were further confirmed by immunofluorescence studies (Fig. 2A), which show both stromal and non-stromal cells internalizing the green fluorescent NPs (200 μg/ml) in live mode.

As reported in the literature, MSCs are the precursors of OBs, and changes at the physiological level affect their osteogenic capability [50]. Therefore, to elucidate the early impacts of NP exposure on the bone marrow niche, we characterized NP uptake, cell viability, and OS responses in human MSCs (HS5) and MM cells (OPM2). Flow cytometry analysis demonstrated a clear dose-dependent internalization of fluorescent NPs, with uptake detectable at concentrations as low as 1 μg/ml and reaching a plateau between 100 and 200 μg/ml after 4 h at 37 °C; uptake was markedly reduced at 4 °C, confirming active endocytic involvement (Fig. 2B). According to our previous work [23] on other components of the bone microenvironment, cell viability assays revealed that HS5 survival remained above 90% at NP concentration up to 50 μg/ml, but declined significantly to 85% and 55% at 100 μg/ml and 200 μg/ml, respectively, after 48 h (Fig. 2C). Correspondingly, reactive oxygen species (ROS) measurements using DCFH-DA staining showed an increasing trend at 100 μg/ml NPs and a significant increase at 200 μg/ml relative to untreated controls, indicating potent OS induction (Fig. 2D).

OPM2 cells exhibited a similar pattern of NP internalization and ROS induction, with uptake kinetics that mirrored HS5 cells (Fig. 2E and G). Viability of OPM2 cells decreased by approximately 20% starting from the lowest concentration of NPs (1 μg/ml) after 48 h (Fig. 2F), suggesting a high sensitivity of tumoral cells to the NP exposure, and proliferation assays revealed a sustained growth arrest from 48 to 96 h post-exposure for all the tested concentrations of NPs (Fig. 2H). At the transcriptional level, quantitative PCR analysis showed a significant upregulation of the antioxidant response gene *HO−1* (350-fold increase) after 48 h of NP exposure followed by 24 h of recovery, while *HSP−60* transcript levels decreased by 40%, suggesting a shift from acute chaperone response to sustained oxidative defense (Fig. 2I–J). Taken together, these findings demonstrate that NP exposure compromises both stromal and malignant cell viability in the bone marrow microenvironment through oxidative stress mechanisms.

3.2. NP-driven alterations in extracellular vesicle biogenesis and incorporation of NPs

Given the central role of EVs in mediating intercellular signaling within the BM in MM, we investigated how NP exposure affects EV biogenesis in OPM2 cells. We first verified the total protein patterns in OPM2 cells, both with and without NP treatment, and in the EVs they released. From the ponceau staining, we observed a slight change in the protein pattern in the EVs derived from cells exposed to NPs compared to those derived from cells not exposed (Supplementary data, Figure S1, A-F). Western blot analysis of EV preparations, normalized by total protein content and GAPDH, revealed modest changes in canonical EV markers CD63, CD81, TSG101, and Histone H3, relative to vesicles from untreated cells (Fig. 3A–C). This shift implies that NP exposure may favor EV release via the endosomal route rather than the plasma membrane budding, suggesting a change in the vesiculation mechanism in response to NPs.

Nanoparticle tracking analysis (NTA) further showed that NP treatment affects the EVs released by OPM2 cells (Fig. 3D-F). Indeed, EVs were smaller, with median diameters shifting from 120 nm in controls to 95 nm in NP exposure, and modal diameters decreasing from 100 nm to 85 nm. Considering that the NPs used in this study possess intrinsic fluorescence within the red channel (ex. 542 nm /em. 612 nm), we conducted an additional analysis to assess the presence of fluorescent particles within the EV population isolated from cells exposed to NPs. Importantly, analyzing the red fluorescence of NP cores, we identified a subpopulation of fluorescent EVs whose size profile overlapped the general distribution, indicating direct NP incorporation into vesicles (Fig. 3F). This finding suggests a potential alteration in EV-mediated intercellular communication, as the presence of NPs within vesicles may interfere with their normal pathophysiological functions, including signal transmission between cells. Such interactions could provide insight into the broader implications of NP exposure on cellular communication and associated processes.

To determine whether these NP-induced alterations extend to other bone marrow-derived cells, we conducted NTA on EVs isolated from MC3T3-E1 pre-osteoblasts after a comparable NP exposure. Similar to OPM2-derived vesicles, NP -exposed MC3T3-E1 EVs displayed a reduction in mean and mode diameters by 15 nm and a 25 % increase in particle number (Table 3).

Taken together, these results suggest that NP exposure profoundly alters the EV population released by OPM2 cells, with likely consequences for their downstream functions.

To determine whether EVs incorporated NPs, we performed spectral flow cytometry analysis using a Cytek Aurora instrument. The NPs used in this study display intrinsic fluorescence in the violet channel (ex. 365 nm/em. 447 nm), which allowed their direct detection. Initially, we profiled the total nanoparticle population and observed that approximately 30% of events within the small-particle gate (defined by FSC-A vs SSC-A, with singlets selected via FSC-H vs FSC-A) exhibited violet

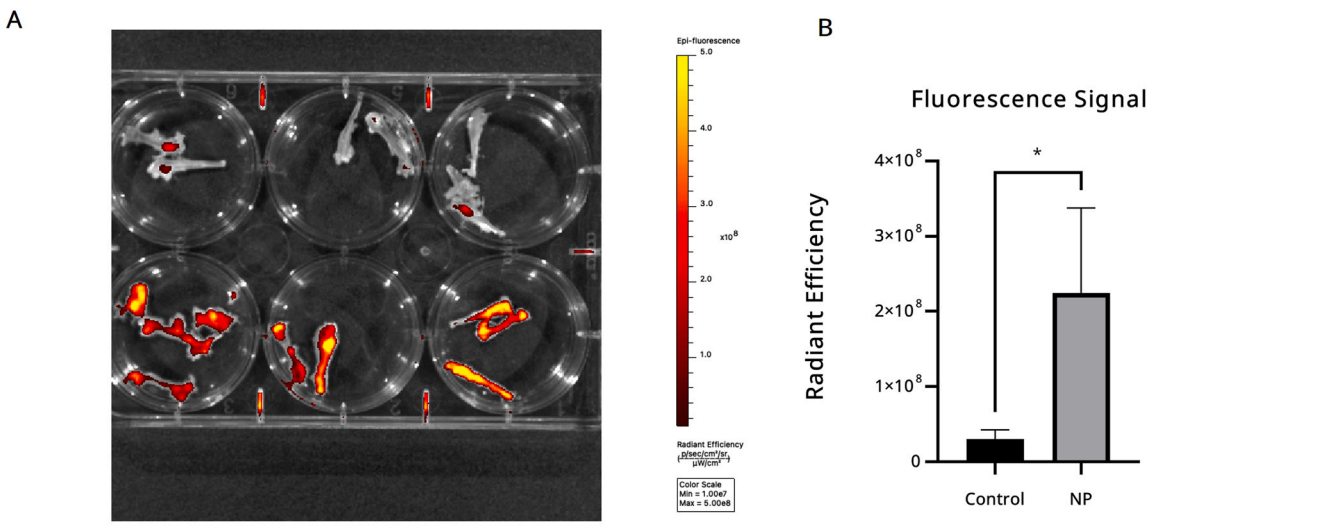

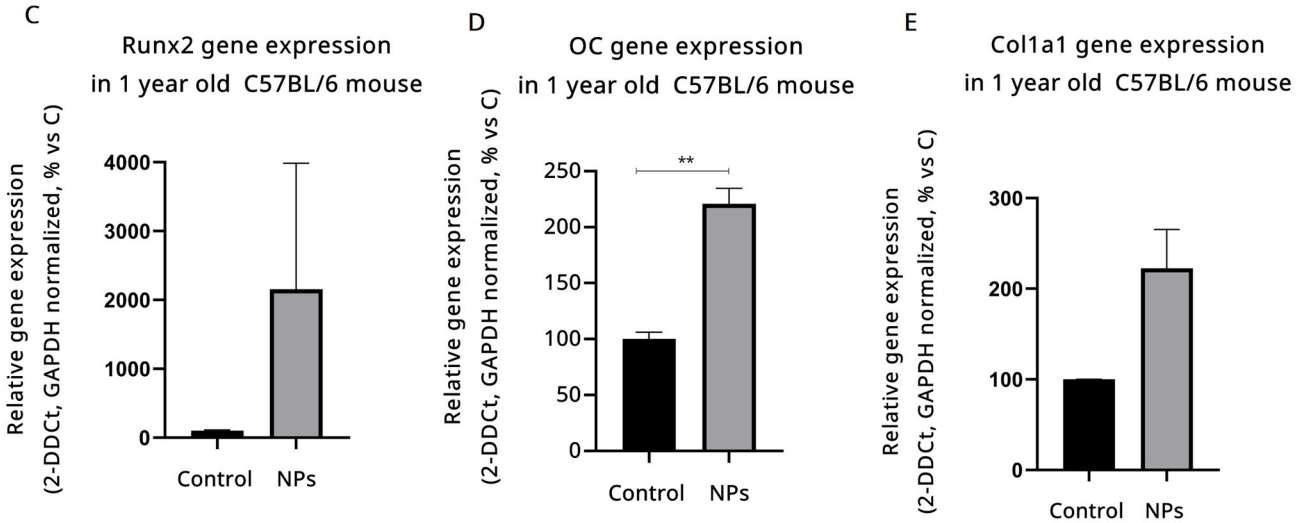

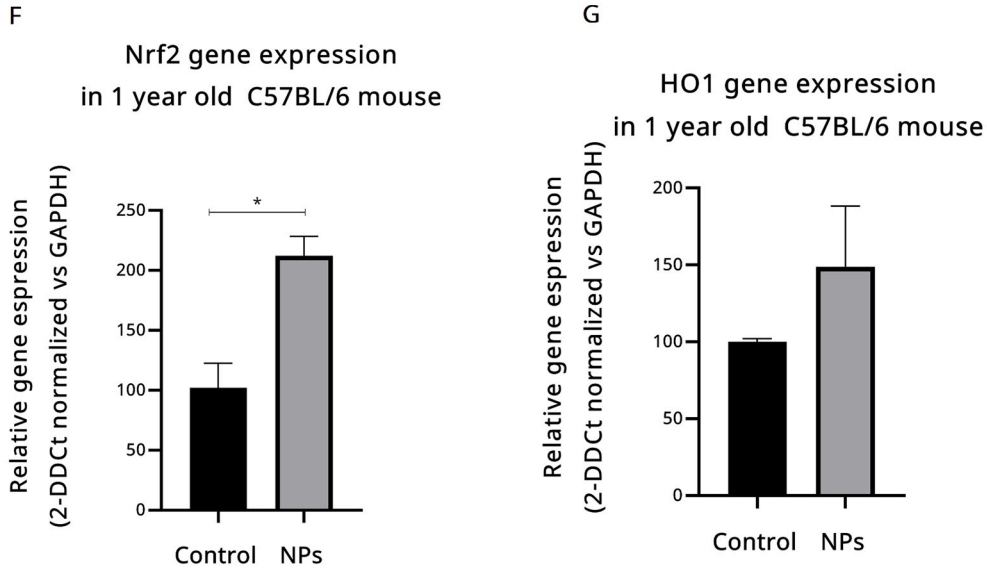

(caption on next page)

Fig. 1. Ex vivo uptake and molecular response to NPs in middle-aged murine bone. (A) Representative IVIS Spectrum fluorescence image of femurs and tibiae isolated from 12-month-old C57BL/6 female mice after 24 h of incubation with either PBS (vehicle control, upper row) or red fluorescent polystyrene nanoplastics (NPs, 50 nm, 200 μg/ml; lower row). (B) Quantification of total radiant efficiency (p/s/cm^2/sr)/(μW/cm^2) indicates significantly increased NP-associated fluorescence in NP-treated bones relative to controls. (C, D, E) Relative RT-PCR analysis of Runx2, Osteocalcin (*OC*), and Collagen 1a1 (*Col1a1*) expression in bone marrow flushed from treated bones. *Runx2, OC, and Col1a1* showed an overall increase in NP-treated samples, with *OC* reaching statistical significance ($p < 0.05$). (F, G) Expression levels of oxidative stress-related genes Nrf2 and Hox1 (*HO−1*), confirming activation of antioxidant pathways in response to NP exposure. The relative mRNA expression was normalized to the housekeeping gene RNA Pol II and calculated by the 2-ΔΔCt formula. Data are shown as mean ± SEM. $p < 0.05$, $p < 0.01$, unpaired *t*-test.

Table 2
Uptake of NPs (parental percentage) in the bone marrow aspirate cellular component.

	Total Viable cells	CD138$^+$/Viable	CD138$^+$/NPs$^+$	CD90$^+$/Viable	CD90$^+$/NPS$^+$	
Control	84,85%	0,71% (vs total viable)	0,23% (vs CD138$^+$/Viable)	0,40% (vs total viable)	0,41% (vs CD90$^+$/Viable)	24 h
NP exposed	86,48%	0,90% (vs total viable)	97,33% (vs CD138$^+$/Viable)	0,48% (vs total viable)	99,95% (vs CD90$^+$/Viable)	

fluorescence, indicating the presence of NPs (Fig. 4A). To refine this analysis and specifically assess whether some of these NP$^+$ events corresponded to structurally intact vesicles, we employed CFSE labeling, a green fluorescent dye (ex. 494 nm/em. 521 nm) that selectively stains intact EVs without overlapping with violet emission (Fig. 4B). By applying a dual gating strategy on CFSE and violet fluorescence, we identified a discrete CFSE$^+$/NP$^+$ population. This double-positive subset represented roughly 10% of the total EV fraction, confirming that a well-defined population of intact vesicles incorporates NPs upon exposure (Fig. 4C). These NP$^+$ EVs also clustered in a lower FSC-A region compared to CFSE$^+$/NP$^-$ EVs, consistent with their reduced size as determined by NTA. This combined approach confirms that, within the broader detection of violet fluorescence across the nanoparticle sample, a specific subset of intact vesicles shows NP internalization. To better characterize the physical changes induced by NPs to EVs and to confirm the data obtained from NTA and flow cytometry, we then analyzed the EVs derived from MM cells (OPM2) exposed to vehicle or NPs at the cryogenic electronic microscopy (Cryo-EM) to obtain EV micrography. From the morphological analysis, it was possible to observe that the EVs derived from cells not exposed to NPs (Fig. 4D) are generally bigger than the EVs derived from OPM2 exposed to NPs (Fig. 4E). Moreover, some EVs exposed to NPs show a different electronic density inside (Fig. 4F): since the electron-dense region covers the total area within the bilayer, we can hypothesize that this population is enriched in NPs covered by a protein corona or lipidic layer.

3.3. Impact of NP exposure on EV cargo and function

Once defined that NP exposure influences the physical characteristics of the EVs released by the cells, we investigated whether the cargo of EVs derived from MM cells exposed to NPs was also changed. To this purpose, we have analyzed the total EV cargo content in terms of miRNAs. The analysis of the amount of ng observed by the specific absorbance indicates a 25% reduction in total miRNA content from NP-derived EVs compared to controls (Fig. 5A).

To explore whether NP exposure affects the molecular machinery involved in miRNA cargo selection, we analyzed the expression of key RNA-binding proteins previously implicated in the selective sorting of miRNAs into EVs. Among these, YBX1 (Y-box binding protein 1) has been reported to mediate the selective loading of specific miRNAs into EVs through RNA-binding and stress-responsive mechanisms [51]. Similarly, hnRNPA2B1 (heterogeneous nuclear ribonucleoprotein A2B1) has been shown to recognize specific sequence motifs in miRNAs and direct their sorting into EVs via sumoylation-dependent pathways [52]. In addition, SYNCRIP (also known as RNPQ) has been identified as a key regulator of miRNA sorting through sequence-dependent binding and EV incorporation [53]. These results indicate that NP exposure is associated with the modulation of multiple components of the miRNA sorting machinery (Fig. 5 B-D).

To identify the miRNAs that could potentially modulate the bone microenvironment in NP exposure conditions, we analyzed total miRNA content in EVs from MM cells (supplementary data) using TaqMan® Low Density Array (TLDA) Human MicroRNA Cards. miRNAs with C_{RT} values > 28, AmpScore < 1.24, or missing amplification were considered not reliably amplified. In Figure S2, we reported the miRNA expression profile as ΔCt values, considering, for eventual validation, miRNAs with a $\Delta Ct \leq 6$. To prioritize candidates for functional validation, we selected EV-associated miRNAs based on reliable expression and biological relevance to either tumor-related pathways or osteogenic regulation. Based on this approach, we validated a panel of candidate miRNAs, including miR−331, miR−216, and miR−766, which are associated with tumor-related processes, as well as miR−505, which has been implicated in osteogenic regulation [54]. While several miRNAs were enriched in EV cargo (Figure S3A-C), we did not observe significant changes in tumor-associated miRNAs upon NP exposure (Figure S3D–F). In contrast, we found an enrichment of miR505 in EV in comparison to cells (Fig. 6A), and, interestingly, we found that its levels were significantly reduced in both cellular (−30%) and EV (−40%) fractions of OPM2 cells exposed to NPs, when compared to control-treated cells (Figs. 6B and 6C). This miRNA has been reported to regulate RUNX2, a key transcription factor controlling osteoblast differentiation, providing a biologically plausible link between EV cargo and the osteogenic phenotype analyzed in our system [54]. Accordingly, MM-EVs inhibited osteoblast differentiation by downregulating Runx2, thereby keeping bone cells in an undifferentiated state [36,55]; moreover, the exposure of pre-osteoblast cells (MC3T3-E1) to MM-EVs significantly reduced Runx2 gene expression, a phenotype potentially related to the action of miR−505, as demonstrated in S4 Figure showing the direct effect of miR−505 mimic on *Runx2* gene expression, both in silico (Figure S4 A) and in the in vitro education model used in our experiments (MM-EVs and MC3T3E1) (Figure S4 B).

The seed sequence of miR−505 is conserved across species, and bioinformatic prediction analyses indicate that the RUNX2 3′UTR contains potential binding sites for miR−505 in both human and murine transcripts. Therefore, despite the cross-species experimental system (human MM cells and murine pre-osteoblasts), miR−505-mediated regulation of RUNX2 remains biologically plausible.

To evaluate whether miR−505 could potentially regulate RUNX2 across species, we analyzed the predicted miR−505 binding sites within the human and murine RUNX2 3′UTR using TargetScan. As shown in Figure S4A, both human and mouse transcripts contain a predicted 7mer-m8 seed-matched site for miR−505 in the human RUNX2 3′UTR and in the murine Runx2 3′UTR. The predicted repression strength is comparable between the two species (context++ score: −0.11 for human and −0.09 for mouse). In addition, the conserved branch length is identical (2.983) for both sites. These features indicate that a predicted miR−505 seed-matched site is present in both human and murine RUNX2 transcripts, supporting the biological plausibility that miR−505

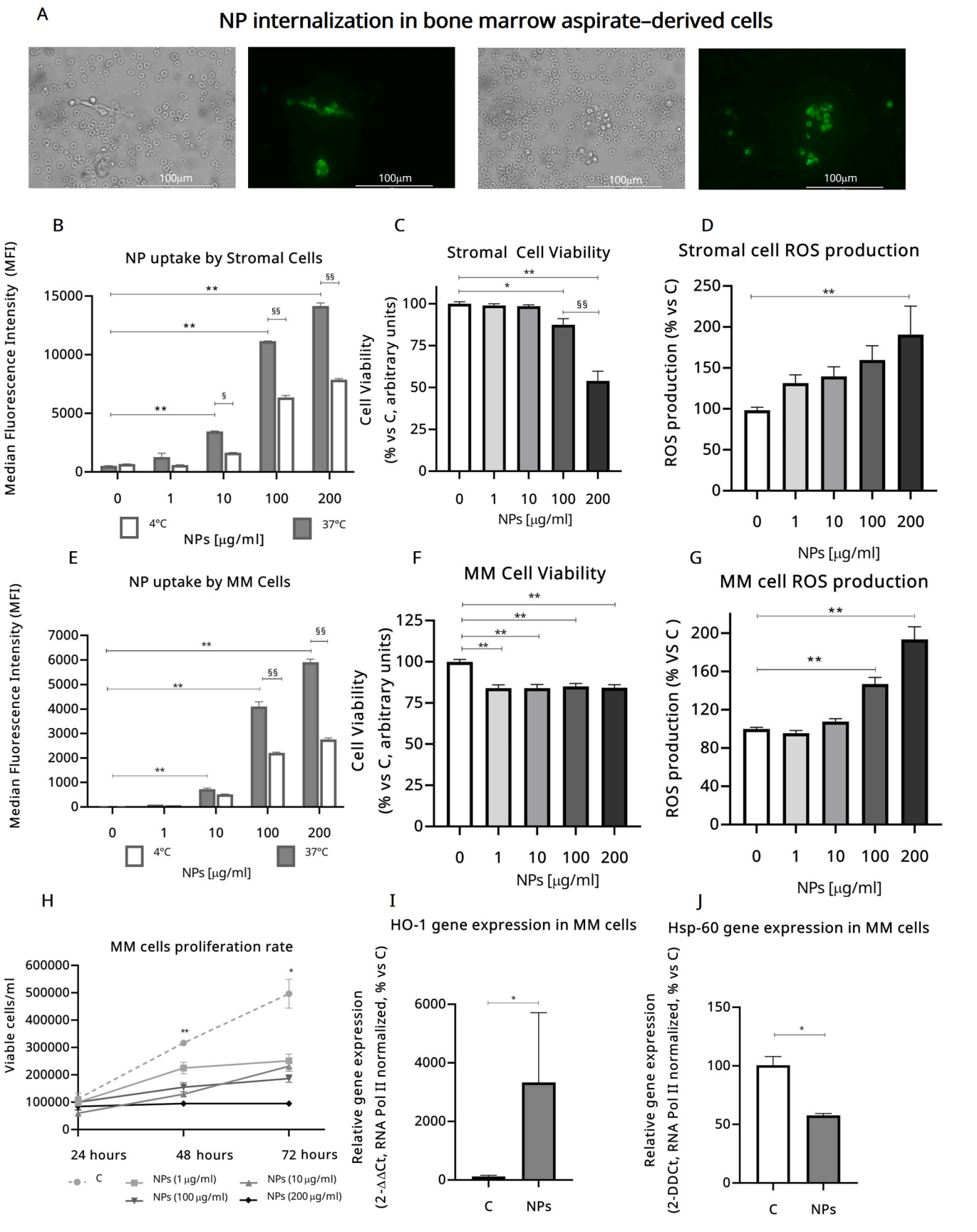

(caption on next page)

Fig. 2. NPs particles induce dose-dependent uptake, cytotoxicity, and oxidative stress in bone marrow microenvironment cells. (A) NPs localize within the bone marrow aspirate cellular compartment. Cells derived from bone marrow aspirates were treated for 24 h with green-NPs at a concentration of 200 μg/ml. Images were obtained under the live imaging mode using an EVOS microscope (40x magnification). (B) Uptake of different concentrations (1–200 μg/ml) of fluorescent NPs in HS5 human mesenchymal stromal cells at 37°C and 4°C after 4 h, assessed by flow cytometry analysis. (C) Viability of HS5 cells was assessed with the MTT assay following a 24-hour exposure to increasing concentrations (1–200 μg/ml) of NPs. (D) Reactive oxygen species (ROS) production in HS5 cells was measured by DCFH-DA staining following a 48-hour exposure to increasing concentrations (1–200 μg/ml) of NPs. (E) Uptake of different concentrations (1–200 μg/ml) of fluorescent NPs in OPM2 multiple myeloma cells at 37°C and 4°C after 4 h, assessed by flow cytometry analysis. (F) Viability of OPM2 cells was assessed with the MTT assay following a 48-hour exposure to increasing concentrations (1–200 μg/ml) of NPs. (G) Reactive oxygen species (ROS) production in OPM2 cells was measured by DCFH-DA staining following a 48-hour exposure to increasing concentrations (1–200 μg/ml) of NPs. (H) Time course (24–72 h) of OPM2 cell proliferation following exposure to increasing concentrations (1–200 μg/ml) of NPs. (I-J) Relative gene expression measured by qPCR of OS-related genes in OPM2 exposed or not to NPs (100 μg/ml) for 48 h. The relative expression of mRNA was normalized to the housekeeping gene RNA Pol II and calculated by the 2-ΔΔCt formula. Statistical analysis was carried out by One-way ANOVA and Tukey post-hoc test. Conditions vs control: * = $p < 0.05$; ** = $p < 0.01$; among conditions §§ = $p < 0,01$.

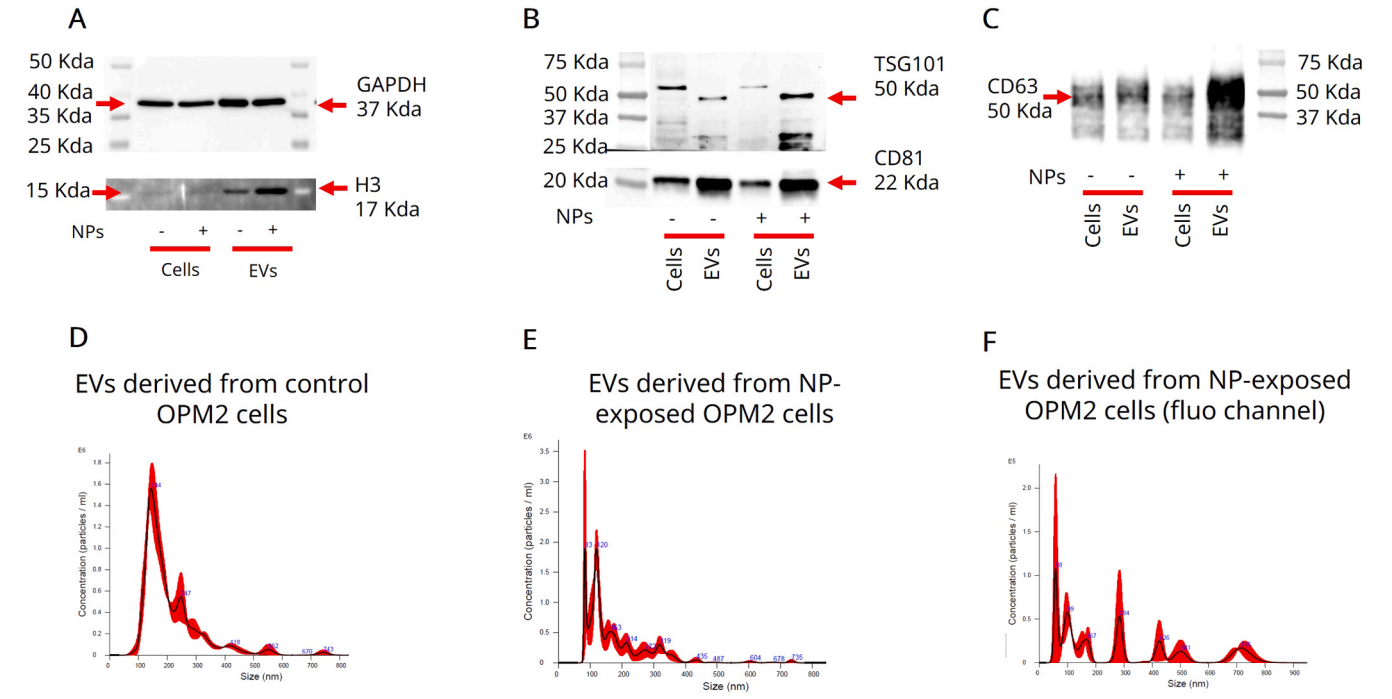

Fig. 3. NP-driven alterations in extracellular vesicle biogenesis. (A-C) Western blot analysis of EV preparations normalized by total protein content, showing canonical EV markers: (A) GAPDH and Histone H3, (B) TSG101 and CD81, and (C) CD63. (D-F) Nanoparticle tracking analysis (NTA) of EVs derived from: (D) control OPM2 cells, (E) NP-exposed OPM2 cells, (F) fluorescent NP-exposed OPM2 cells (ex. 542 nm / em. 612 nm) identifying a subpopulation of red fluorescent EVs with size profiles overlapping the general distribution, indicating direct incorporation of NPs into vesicles. These findings suggest that NP exposure not only alters EV biogenesis mechanisms but also results in NP-containing vesicles that may disrupt normal intercellular communication within the bone marrow microenvironment.

Table 3
EVs analysis parameter in OPM2 and MC3T3-E1 cells.

Cells	Parameter	MM-EVs	MM-NP-EVs	MM-NP-EVs (fluo channel)
OPM2	Mean ± SEM (nm)	225,81 ± 10,50	176,47 ± 12,51	151,36 ± 27,85
	Mode ± SEM (nm)	133,24 ± 7,27	96,31 ± 8,28	66,83 ± 5,93
	[C] ± SEM (particle/ml)	9,53E + 07 ± 1,57E + 07	6,03E + 08 ± 2,03E + 08	4,44E + 07 ± 2,36E + 07
MC3T3-E1	Mean ± SEM (nm)	204,38 ± 11,51	137,33 ± 5,00	-
	Mode ± SEM (nm)	147,78 ± 18,18	86,47 ± 3,70	-
	[C] ± SEM (particle/ml)	7,03E + 07 ± 1,02E + 07	2,47E + 08 ± 6,16E + 07	-

derived from human MM cells could interact with murine Runx2 in osteoprogenitor cells. We confirmed this in silico analysis, treating MC3T3-E1 cells with EVs derived from NP-exposed OPM2 cells in the presence of a miR−505 mimic. The addition of the miR−505 mimic in the presence of MM-EVs partially restored the inhibitory effect on Runx2 gene expression, as expected from the literature. These findings suggest that miR−505 contributes, at least in part, to the regulation of RUNX2 expression mediated by MM-derived EVs (Figure S4, panel B).

As a functional test, we treated MC3T3-E1 pre-osteoblasts with equal numbers of EVs from control or NP-exposed OPM2 cells. While control EVs induced a 25% decrease in *Runx2* mRNA expression (Fig. 7A) and in *Runx2* target genes involved in osteoblastogenesis, such as *osteocalcin* (*OC*) (Fig. 7B) and *collagen 1a1* (*Col1a1*) (Fig. 7C), NP-EVs elicited no significant change, consistent with a reduced miR−505-dependent contribution (Fig. 7A-C). This is further supported by the calcification assay with alizarin red S, which shows a corresponding functional trend in mineral deposition in pre-osteoblasts exposed to EVs from NP-treated cells (Fig. 8A–B). These findings suggest that NPs affect the capability of the MM-EVs to educate the bone microenvironment and that this alteration is partially mediated by miR−505 modulation.

Taken together, these findings indicate that NP exposure alters EV cargo composition and is associated with a reduced contribution of miR−505 to EV-mediated regulation of osteogenic signaling, revealing a novel pathway through which environmental particles perturb bone

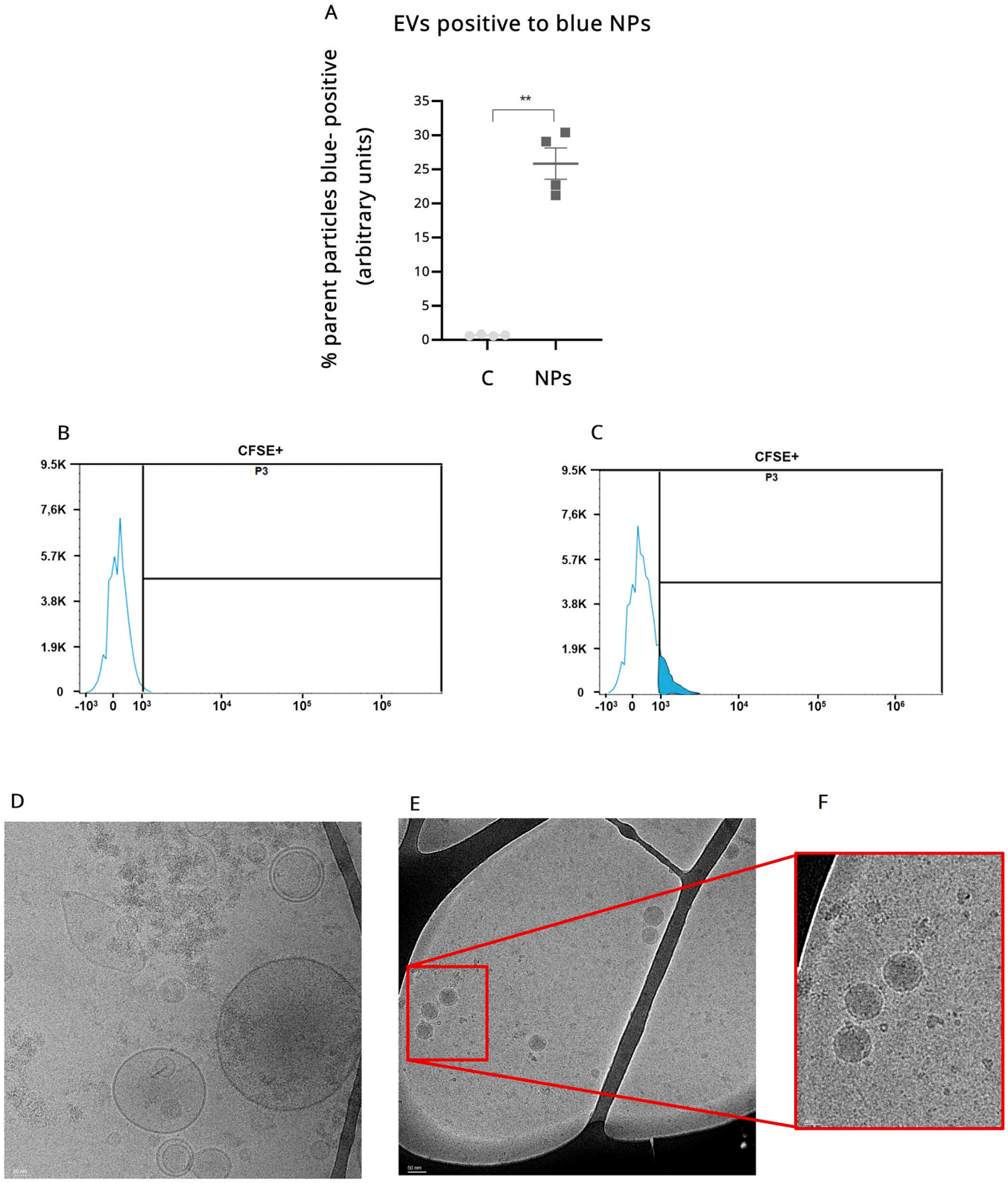

Fig. 4. NP-exposed OPM2 cells produce EVs incorporating NPs. EVs released by OPM2 cells exposed to vehicle (Control) or blue-fluorescent NPs were labeled with CFSE (ex. 494 nm/em. 521 nm) to mark intact vesicles, then analyzed on a Cytek Aurora. (A) Quantification of the percentage of nanoparticles that fall within the NP-positive fluorescence gate (V4 detector) for control and NP-treated samples (B). Histogram of violet-channel (V4) fluorescence intensity for $CFSE^+$ EVs isolated from control-treated OPM2 cells, showing the distribution of CFSE signal with minimal spillover in the violet wavelength. (C) Histogram of violet-channel (V4) fluorescence intensity for $CFSE^+$ EVs isolated from NP-treated OPM2 cells, illustrating the shift in fluorescence corresponding to NP incorporation. Statistical analysis was carried out using one-way ANOVA and the Tukey post-hoc test. Conditions vs control: ** = $p < 0.01$. (D–F) Cryo-electron micrographs of EVs from OPM2 cells treated with vehicle (D) or NPs (E–F). NP-EVs appear smaller and more homogeneous in diameter (E) than control EVs (D), and a subset displays an electron-dense core filling the vesicle lumen (F), indicative of NPs enveloped by a protein/lipid corona. Scale bars: 100 nm.

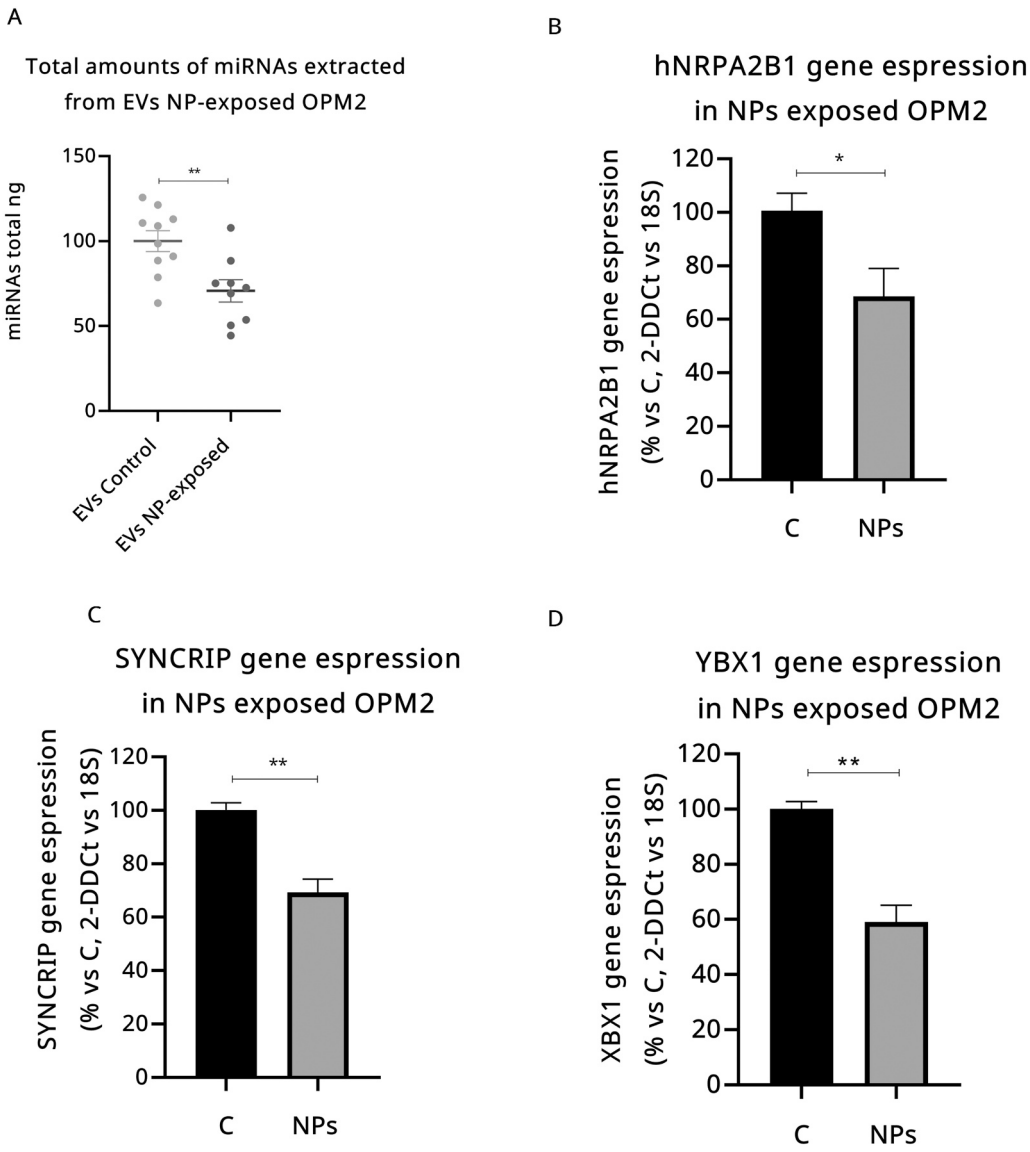

Fig. 5. Exposure of cells to NPs affects MM-EV cargo. (A) Total miRNA content of EVs derived from cells exposed to NPs or to the vehicle (control). (B) mRNA expression of hnRNPA2B1 in OPM2 cells exposed to NPs or to the vehicle. (C) mRNA expression of SYNCRIP in OPM2 cells exposed to NPs or to the vehicle. (D) mRNA expression of YBX1 in OPM2 cells exposed to NPs or to the vehicle.

marrow intercellular communication not only in a physiological setting but also in pathological conditions.

4. Discussion

Multiple myeloma predominantly affects elderly individuals, with a median age at diagnosis of approximately 70 years. In this context, the age-associated bone marrow microenvironment represents a pathophysiologically relevant system in which to explore microenvironmental dynamics. Age-associated changes (such as increased bone marrow adiposity, elevated pro-inflammatory cytokines (e.g., IL−6), stromal functional alterations, and impaired osteoblastogenesis) mirror key features of the MM-permissive niche [43,49]. To capture this complexity, we used 12-month-old murine bones as a middle-aged *ex vivo* bone model to explore the early impact of NP exposure. Importantly, the NP concentration used in the *ex vivo* bone immersion assay should be interpreted as a high-dose mechanistic challenge designed to test tissue permissiveness, nanoparticle retention, and early molecular responsiveness, rather than as a direct surrogate of physiological exposure within the bone marrow compartment. Accordingly, the present work should be interpreted as a mechanistic proof-of-concept study designed to investigate EV-mediated responses to nanoplastic exposure, rather than as a quantitative environmental exposure model. In this context, the experimental setup was specifically designed to interrogate early EV-associated molecular responses to nanoplastic exposure in a controlled microenvironment, allowing mechanistic dissection of acute nanoparticle-induced perturbation independently of long-term accumulation or systemic exposure variables. Although our *ex vivo* exposure condition does not reproduce physiological marrow concentrations, recent human studies support the biological plausibility of skeletal and marrow exposure to plastic particles. Microplastics have been detected in human skeletal tissues, including bone, cartilage, and intervertebral discs [56], and independent analyses have reported microplastic deposition within human bone marrow [20], raising concern about potential interactions with hematopoietic and stromal compartments. These findings support the biological plausibility that plastic particles may interact with bone marrow-associated compartments, while also underscoring the need for quantitative exposure studies. NP-treated bone specimens showed robust NP retention, coupled with transcriptional upregulation of osteogenic genes including *Runx2, OC, and*

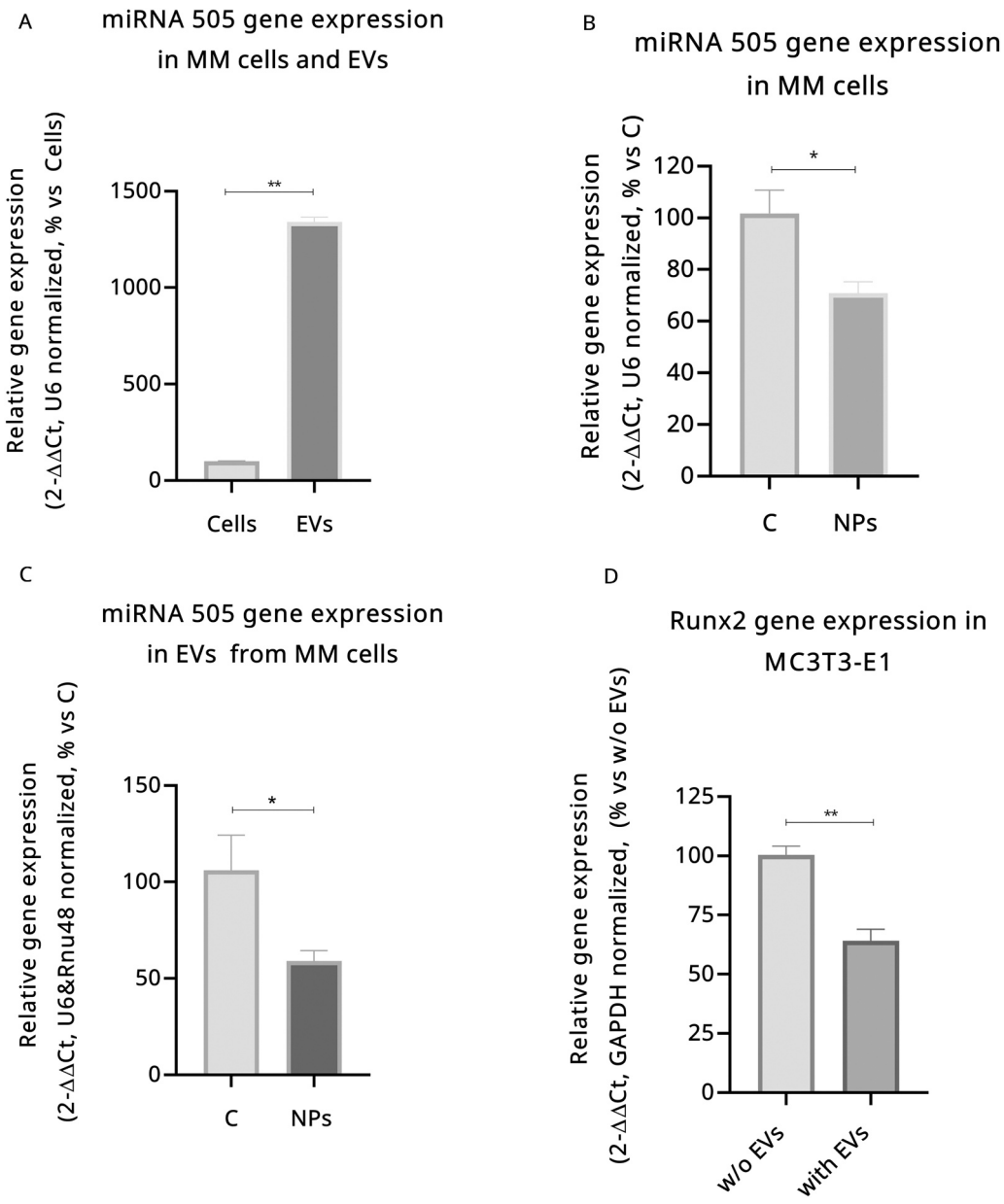

Fig. 6. Exposure of cells to NPs alters miR−505 expression and MM-EV education. (A) miRNA−505 expression in OPM2 cells and in OPM2-derived EVs. (B) miRNA−505 expression in OPM2 cells exposed to NPs or to the vehicle. (C) miRNA−505 expression in OPM2-derived EVs exposed to NPs or to the vehicle. (D) mRNA expression of Runx2 in MC3T3-E1 cells treated with vehicle (w/o EVs) or with OPM2-derived EVs. Data are expressed as the mean value (±SEM) of at least three independent experiments (3 replicates for each experiment). Statistical analysis was performed by ANOVA and the Tukey post-hoc test. Conditions vs control: * = $p < 0.05$; ** = $p < 0.01$.

Col1a1. These were accompanied by increased expression of oxidative stress response genes such as *Nrf2* and *HO−1*. Notably, these gene signatures are consistent with an acute transcriptional response involving osteogenic and antioxidant pathways, rather than evidence of sustained anabolic effect [57] likely reflect a short-term priming response by the middle-aged bone niche to acute NP-induced oxidative and inflammatory stress. To validate and extend these observations into a clinically relevant context, we turned to human MM bone marrow. Using medullary aspirates from an MM patient, we demonstrated nearly complete uptake of fluorescent NPs by both CD90 + stromal cells and CD138 + malignant plasma cells after 24 h of exposure. Immunofluorescence imaging confirmed NP internalization across both stromal and non-stromal compartments. These data demonstrate that human MM-derived bone marrow cells are permissive to NP uptake under experimental conditions. Hence, to better elucidate the functional impact of NP exposure on the bone marrow niche, we performed a series of *in vitro* experiments using MM and stromal cell lines. In particular, having demonstrated NP retention in murine bone tissue and NP uptake by human MM bone marrow cells, we next examined their downstream consequences on BM cell populations and their intercellular communication via extracellular vesicles. The *in vitro* studies corroborated the evidence that NPs perturb the BM microenvironment by inducing OS and by affecting the viability of cells under the pathological conditions of MM. In addition to compromising cell survival, NPs significantly altered the vesiculation process, leading to an increased release of EVs with a reduced diameter compared to those derived from cells not exposed to NPs. This size alteration was associated with changes in the EV cargo, which may affect their ability to regulate intercellular communication within the bone marrow microenvironment. Importantly, these effects are independent of a tumoral phenotype, as they

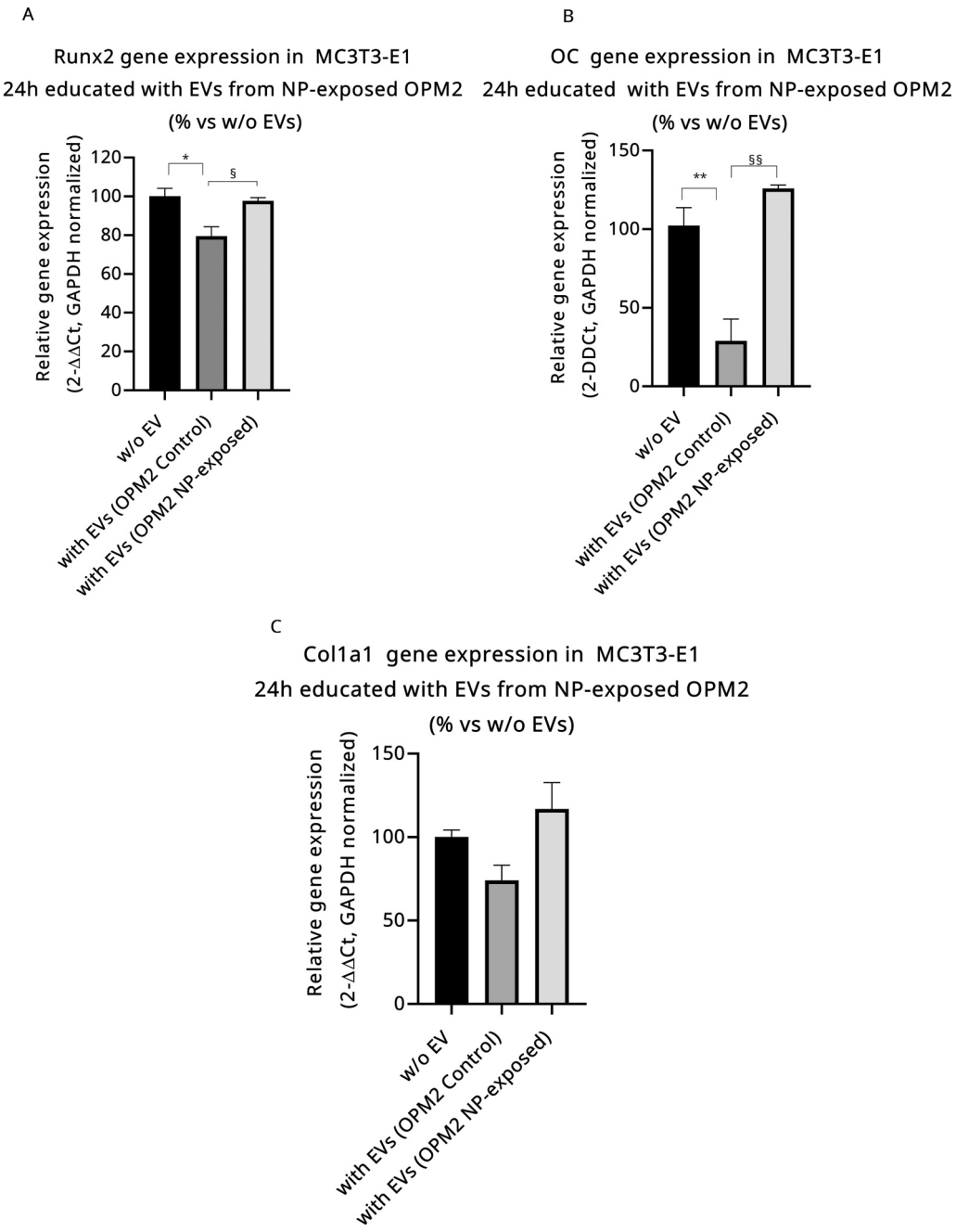

Fig. 7. Exposure of cells to NPs affects the education of pre-osteoblast cells. (A) mRNA expression of Runx2 in MC3T3-E1 cells treated with EVs released by vehicle-treated or by NP-exposed OPM2 cells. (B) mRNA expression of OC in MC3T3-E1 cells treated with EVs released by vehicle-treated or by NP-exposed OPM2 cells. (C) mRNA expression of Col1a1 in MC3T3-E1 cells treated with EVs released by vehicle-treated or by NP-exposed OPM2 cells. Data are expressed as the mean value (±SEM) of at least three independent experiments (3 replicates for each experiment). Statistical analysis was performed by ANOVA and Tukey post-hoc test. Conditions vs with EV: * = $p < 0.05$; ** = $p < 0.01$, vs with EV OPM2 (control): § = $p < 0.05$; §§ = $p < 0.01$.

were consistently observed in pre-osteoblasts and MM cells. These findings suggest that NPs interfere with the physiological mechanisms of EV biogenesis and cargo loading, potentially disrupting the EV-mediated crosstalk, which is crucial for maintaining bone homeostasis.

The bone microenvironment plays a central role in MM progression and relapse. Bone remodeling dynamics create a niche that supports MM cell survival and contributes to disease persistence [30]. In this context, malignant plasma cell-derived EVs are particularly relevant because they actively condition the bone compartment. Tumor-derived EVs are known to modify the microenvironment to promote cancer-supportive functions [51]. In MM, EV-mediated suppression of osteoblast differentiation contributes to the maintenance of an osteoblast-suppressive, tumor-permissive niche, in part by modulating Runx2-dependent osteogenic signaling [50].

To better contextualize these findings, it is important to consider the emerging role of EVs as dynamic targets of environmental perturbation. EVs are not only key mediators of intercellular communication, but also highly responsive structures whose biogenesis, release, and cargo composition are tightly regulated by cellular stress conditions. Increasing evidence indicates that environmental stressors, including nanoparticles, can directly affect EV biology by altering vesicle formation, size distribution, and molecular cargo, including proteins and miRNAs [39,40]. In this context, EVs represent a critical interface between intracellular responses to external stimuli and the modulation of

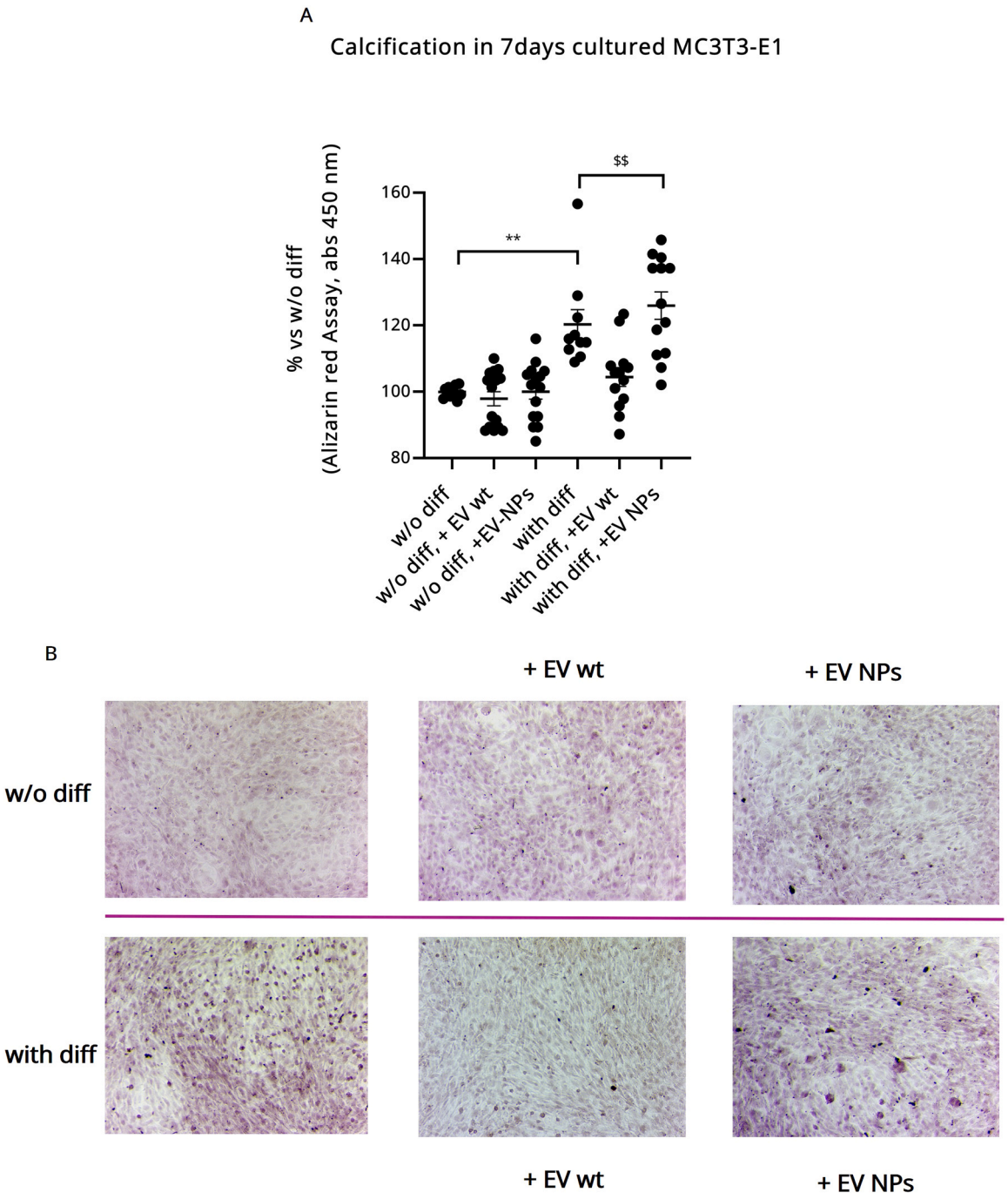

Fig. 8. Exposure of cells to NPs affects calcium deposition. (A) Calcium deposition level in cells cultured for 7 days, differentiated to osteoblasts or not, and treated with EVs released by vehicle-treated or by NP-exposed OPM2 cells exposed to NPs. (B) Micrographs of MC3T3E−1 cells stained with Alizarin Red S and differentiated to osteoblasts or not, and treated with EVs released by vehicle-treated or by NP-exposed OPM2 cells exposed to NPs.

extracellular signaling networks. Recent studies have shown that engineered and environmental nanoparticles can influence EV biogenesis and selectively modulate cargo loading [58], while also being incorporated into EVs, suggesting a bidirectional interaction between these systems [38]. Taken together, these observations position EVs as both mediators and biologically relevant targets of nanoparticle-induced perturbations, providing a mechanistic framework to understand how nanoplastics may reshape intercellular communication within complex biological systems, including the tumor microenvironment [30,55,59]. Our results confirm that NPs interfere with this regulatory mechanism by altering the molecular cargo of EVs, potentially weakening their ability to suppress osteoblast differentiation and thereby influencing bone remodeling in the context of MM. Specifically, EVs derived from NP-exposed MM cells showed a reduced ability to repress Runx2 and its downstream targets in pre-osteoblasts, consistent with the observed depletion of miR−505.

Our results show that NP exposure modulates multiple components of the miRNA sorting machinery. Since the role of these proteins (*YBX1, hnRNPA2B1, SYNCRIP*) in regulating the selective incorporation of miRNAs into EVs is well established, and also their modulation in response to stress (see Park, [60]), their downregulation may contribute to the altered EV cargo composition observed under NP exposure conditions, including the possible reduction of miR−505 levels. However, although NP exposure induces specific alterations in EV biogenesis and

cargo, we cannot exclude that part of the observed miRNA changes reflects a broader oxidative stress response rather than a nanoplastic-specific mechanism. In this context, the reduction of EV-associated miR−505 is best interpreted as a contributing factor to the observed modulation of osteogenic signaling, rather than as a single causal determinant. This interpretation is consistent with the central role of oxidative stress as an upstream regulator of EV remodeling.

Given the established link between cellular stress and EV biogenesis [61], it is likely that the OS induced by NPs plays a central role in driving these changes in EV cargo and release dynamics [39]. OS not only increases the number of EVs released but also modulates their biochemical composition [61]. For example, cells exposed to chemotherapeutic agents secrete EVs enriched with oxidized and ubiquitylated proteins as a detoxification mechanism. Similarly, environmental stressors such as hyperoxia and hypoxia alter the miRNA composition of EVs, with potential consequences for the behavior of recipient cells [61].

Consistent with these findings, we previously demonstrated that NPs induce OS and reduce cell viability in both stromal and MM cells. These results align with other reports showing that NPs increase ROS production and trigger inflammatory responses, ultimately disrupting the balance of bone remodeling [23].

At the molecular level, exposure to NPs induces changes in gene expression that reflect an attempt to counteract OS. In MM cells exposed to NPs, we observed upregulation of *HO−1*, a known target of the Nrf2 antioxidant pathway [62], suggesting that these cells initiate a defensive response against ROS accumulation. Concurrently, we detected a downregulation of HSP60, a chaperone protein typically overexpressed in tumors to promote cell survival and resistance to apoptosis [63]. This reduction in *HSP60* may explain the decrease in MM cell viability and proliferation observed following NP exposure. These findings highlight a dual cellular response: an attempt to mitigate oxidative damage while experiencing a reduction in key survival mechanisms.

Our data further indicate that NPs influence EV biogenesis by modifying the composition of released vesicles. According to the MISEV 2023 guidelines, EVs can be classified based on specific protein markers that reflect their cellular origin and pathway of formation [64]. In our study, EVs derived from NP-exposed cells showed a slight enrichment of CD81, a transmembrane protein associated with plasma membrane-derived EVs. In contrast, EVs from NP-exposed cells exhibited higher levels of TSG101 and CD63, a marker indicative of the endosomal pathway. This shift suggests that NP exposure may favor EV release through the endosomal route rather than the plasma membrane budding. Similar alterations in EV biogenesis have been reported following nanomaterial exposure in other cellular contexts [40], reinforcing the idea that NPs disrupt normal vesiculation processes. Indeed, our study focused on polystyrene nanoplastics, but other nanomaterials, such as metallic, carbon-based, or alternative polymeric nanoparticles, have also been shown to induce oxidative stress and influence EV biogenesis and cargo composition [40]. However, the long-term persistence and physicochemical stability of plastic-derived NPs may render their effects particularly relevant in the bone microenvironment, where structural constraints and cellular turnover are slower compared to other tissues [65,66].

Morphological differences between EVs from NP-exposed and control cells further support the notion of NP-induced changes in vesicle biogenesis. EVs from control cells exhibited a multilayered structure, while those from NP-exposed cells were smaller, spherical, and likely surrounded by a monolayer (either lipidic or proteinaceous). Recent cryo-electron microscopy studies have identified multilayered EVs with complex lipid bilayers [67], raising intriguing questions about the relationship between EV structure and function. A likely contributor to these structural differences is the formation of a protein corona—a layer of adsorbed proteins surrounding NPs upon contact with biological environments [68,69]. This corona may influence both the physical properties of EVs and their biogenesis pathway.

The functional consequences of these NP-induced changes in EV biogenesis and structure become particularly evident when analyzing with flow cytometry the incorporation of NPs into EVs and the resulting alterations in their physical characteristics. Indeed, approximately 20% of EVs from NP-exposed cells contained a detectable NP signal, while the remaining EV population exhibited reduced size compared to control-derived EVs. These results suggest that NP exposure triggers a vesiculation response aimed at eliminating NPs through the EV pathway. Consistent with our findings, previous studies have shown that OS induced by nanomaterials increases EV production and alters their molecular composition [40,70,71]. In addition to modifying EV biogenesis, NPs also affect EV cargo. We observed a significant reduction in both total miRNA content and the specific levels of miR−505 in EVs from NP-exposed MM cells. Since miR−505 is a known regulator of *Runx2* expression, its depletion may impair the ability of MM-EVs to suppress osteoblast differentiation [54]. This suggests that NP-induced changes in EV cargo may weaken the pro-tumorigenic influence of MM-EVs by diminishing their ability to maintain an undifferentiated bone microenvironment— a condition that is otherwise favorable for MM progression [55]. Interestingly, while our *in vitro* EV data show a reduced suppression of osteogenic programs in pre-osteoblasts, the *ex vivo* NP-treated middle-aged bones exhibit a direct upregulation of osteogenic and antioxidant genes. At first glance, this may appear inconsistent; however, these phenomena can be reconciled by considering the nature and timing of the response. The *ex vivo* setting reflects an immediate, intact tissue response to NP exposure, characterized by inflammatory priming and compensatory upregulation of osteogenesis. Conversely, the *in vitro* system isolates the effect of altered EV signaling over time. Thus, the *ex vivo* and *in vitro* findings likely reflect distinct layers of response: an acute tissue-level transcriptional response to NP exposure and a cell communication-level alteration mediated by EV remodeling.

Based on these findings, we propose the hypothesis that NPs, by inducing OS and altering EV biogenesis and miRNA sorting, disrupt the mechanisms through which MM cells manipulate their microenvironment. In the context of MM, tumor-derived EVs contribute to maintaining an osteoblast-suppressive bone state that supports a tumor-permissive niche. Our data suggest that NP exposure may interfere with this process by reducing the levels of specific regulatory molecules, such as, at least in part, miR−505, within EVs. This disruption may attenuate the EV-mediated suppression of osteogenic signaling, thereby altering the balance of communication within the bone marrow niche. Moreover, the shift in EV biogenesis pathways indicates that NPs could induce alternative vesiculation mechanisms that affect how MM cells interact with surrounding cells. By promoting the release of smaller vesicles and facilitating the elimination of cellular stress products, NPs may interfere with the finely tuned EV-mediated signaling required to sustain a permissive microenvironment for MM cell survival. These molecular and structural changes, combined with the observed reduction in cell viability, suggest that NP exposure perturbs selected components of MM-driven bone marrow communication, without implying a net beneficial effect on bone remodeling.

Importantly, the reduced ability of EVs from NP-exposed MM cells to suppress osteogenic signaling should not be interpreted as a beneficial effect of nanoplastic exposure. In the context of multiple myeloma, EV-mediated inhibition of osteoblast differentiation represents a key mechanism sustaining a tumor-permissive niche. Therefore, the observed effect reflects a disruption of pathological intercellular communication, rather than a restoration of physiological bone homeostasis. This interpretation is further supported by the fact that NP exposure is associated with oxidative stress, altered EV biogenesis, and broader perturbation of bone marrow cell function, which are generally consistent with detrimental rather than therapeutic biological effects. At the same time, it remains unclear whether these EV-associated changes are fully specific to nanoplastics or reflect, at least in part, a broader stress-adaptive response. EV biogenesis and cargo loading are known to be highly responsive to oxidative and cellular stress, and other

environmental stressors may similarly alter tumor-derived EV function. However, the coordinated modulation of miRNA-sorting regulators, selective cargo alterations, and functional rescue data observed in our study support a structured remodeling of EV-mediated signaling rather than a purely stochastic or passive effect. The broader implications of these alterations on the bone microenvironment remain complex, as NPs simultaneously induce oxidative damage that could impair normal bone homeostasis, and perturb cell-to-cell signaling. Moreover, the observation that a subset of EVs incorporates nanoplastic material raises the possibility that EVs may participate in nanoparticle trafficking within biological systems. In this framework, EVs could act as carriers of internalized nanoplastics, potentially facilitating their intercellular transfer and distribution. This "Trojan horse"–like mechanism has been proposed for other classes of nanomaterials and suggests that vesicular encapsulation may influence nanoparticle fate by shielding them from direct extracellular interactions [72]. However, the extent to which EV-mediated transport contributes to nanoparticle dissemination in vivo remains to be determined and warrants further investigation. These multiple effects align with emerging evidence that nanomaterials can modulate EV-mediated communication to alter tumor progression and metastasis [73,74]. Overall, our data support a model in which nanoplastic exposure perturbs EV-mediated communication within the multiple myeloma bone marrow microenvironment through oxidative-stress-associated remodeling of EV biogenesis and cargo. These findings provide a mechanistic basis for future *in vivo* studies aimed at determining how environmental particle exposure influences bone marrow niche signaling and disease-relevant interactions.

5. Conclusion

This study provides mechanistic insight into how polystyrene nanoplastics can perturb cellular crosstalk within the bone marrow microenvironment. Using complementary *ex vivo* and *in vitro* models, we demonstrate that NPs are efficiently internalized by middle-aged murine bone tissue and by human MM-derived bone marrow cells, where they induce oxidative stress and alter EV-mediated communication. Importantly, our findings identify extracellular vesicles as a previously underappreciated and highly sensitive target of nanoplastic exposure. We show that NP exposure affects EV biogenesis, vesicle-associated cargo, and miRNA sorting, ultimately reducing the ability of MM-derived EVs to modulate osteogenic signaling in recipient pre-osteoblasts. These results provide a mechanistic link between environmental nanoparticle exposure and the disruption of intercellular communication within a disease-relevant bone marrow niche. These alterations should not be interpreted as beneficial for MM-associated bone disease, but rather as evidence that environmental particles can interfere with pathological signaling networks that regulate tumor–stroma interactions. In this context, our study highlights the possibility that nanoplastics act as modifiers of microenvironmental communication, with potential implications for conditions already characterized by oxidative stress, inflammation, and impaired bone remodeling. Although direct clinical evidence on NP effects in humans remains limited, the detection of micro- and nanoplastics in blood and skeletal tissues supports the biological plausibility that environmental nanoplastics may access bone-associated compartments. While our data do not establish *in vivo* functional outcomes or predict the net impact of chronic NP exposure on bone remodeling or MM progression, they define EV-mediated signaling as a critical interface through which environmental perturbations may influence bone marrow niche dynamics.

Overall, this work advances the current understanding of nanoplastic–cell interactions by moving beyond cytotoxicity and identifying EV remodeling as a mechanistically relevant layer of regulation. These findings provide a conceptual and experimental framework for future studies aimed at determining the *in vivo* consequences of nanoplastic exposure and at dissecting the molecular pathways linking oxidative stress, EV biology, and tumor–microenvironment communication. Future investigations integrating transcriptomic and proteomic profiling of EVs and bone marrow tissues will be essential to identify the signaling networks involved in NP-induced remodeling, including pathways such as Nrf2-mediated antioxidant responses and Notch-dependent intercellular signaling.

Environmental implications

Nanoplastics are emerging contaminants found across all environmental compartments. They are generated through the weathering, degradation, and fragmentation of larger plastic debris. Due to their extremely small size, nanoplastics can interact with living organisms—including humans—at various levels of biological organization, penetrating cells and potentially disrupting multiple cellular pathways. However, current knowledge regarding their toxicological impact on organisms and human health remains limited. This study investigates, under controlled experimental conditions, how nanoplastics can perturb extracellular vesicle-mediated communication within the bone marrow microenvironment of multiple myeloma. Although the exposure conditions used here are mechanistic rather than environmentally quantitative, the findings identify EV-mediated signaling as a sensitive biological target of nanoplastic-induced stress and provide insight into how emerging contaminants may interfere with tumor–microenvironment communication.

CRediT authorship contribution statement

Alessandro Villa: Writing – review & editing, Writing – original draft, Methodology, Investigation, Conceptualization. **Beatrice De Felice:** Writing – review & editing, Investigation. **Mauro Turrini:** Resources. **Francesca Guidotti:** Resources. **Martina Chiu:** Writing – review & editing, Conceptualization. **Valentina Citro:** Writing – review & editing, Methodology, Investigation, Conceptualization. **Marco Parolini:** Writing – review & editing, Writing – original draft, Funding acquisition, Formal analysis, Conceptualization. **Giulia Sauro:** Writing – review & editing, Writing – original draft, Investigation, Data curation. **Lavinia Casati:** Writing – review & editing, Writing – original draft, Resources, Investigation, Funding acquisition, Formal analysis, Data curation, Conceptualization. **Paolo Ciana:** Writing – review & editing, Supervision, Funding acquisition. **Raffaella Chiaramonte:** Writing – review & editing, Conceptualization. **Domenica Giannandrea:** Writing – review & editing, Investigation. **Natalia Platonova:** Writing – review & editing, Investigation. **Elena Lesma:** Writing – review & editing, Formal analysis. **Clara Bernardelli:** Writing – review & editing, Investigation.

Funding

Open access provided by Università degli Studi di Milano within the CRUI-CARE Agreement. This research was funded by Linea 2 Università degli Studi di Milano (Department of Health Science), by PRIN2022C5RHRT and PRIN P2022RSWWF funded by Next Generation EU and MUR, to L.C., M.P., and M.C. Figures were created with BioRender.com (License RK28KCESYE), purchased by the University of Milan.

Declaration of Competing Interest

The authors declare that they have no known competing financial interests or personal relationships that could have appeared to influence the work reported in this paper.

Acknowledgement

We gratefully acknowledge NOLIMITS, the advanced imaging facility established by the Università degli Studi di Milano, for contributing

to this work. We also thank the CRC Nano/microplastics on Environments, Medicine, Ecology, Systems Interaction Studies – NEMESIS, Università degli Studi di Milano. We gratefully acknowledge Dr. Bevilacqua from TÜV Rheinland, Dr. Gloria Sini, and Dr. Elisabetta Calzavara from Valduce Hospital for their support.

Appendix A. Supporting information

Supplementary data associated with this article can be found in the online version at doi:10.1016/j.jhazmat.2026.142667.

Data availability

Data will be made available on request.

References

[1] da Costa, J.P., Santos, P.S.M., Duarte, A.C., Rocha-Santos, T., 2016. Nano)plastics in the environment - Sources, fates and effects. Sci Total Environ 566-567, 15–26.
[2] Klaine, S.J., Koelmans, A.A., Horne, N., Carley, S., Handy, R.D., Kapustka, L., Nowack, B., von der Kammer, F., 2012. Paradigms to assess the environmental impact of manufactured nanomaterials. Environ Toxicol Chem 31 (1), 3–14.
[3] Gigault, J., Halle, A.T., Baudrimont, M., Pascal, P.Y., Gauffre, F., Phi, T.L., Hadri, H.El, Grassl, B., Reynaud, S., 2018. Current opinion: what is a nanoplastic? Environ Pollut 235, 1030–1034.
[4] Ter Halle, A., Ghiglione, J.F., 2021. Nanoplastics: a complex, polluting terra incognita. Environ Sci Technol 55 (21), 14466–14469.
[5] Carr, S.A., Liu, J., Tesoro, A.G., 2016. Transport and fate of microplastic particles in wastewater treatment plants. Water Res 91, 174–182.
[6] Tosin, M., Weber, M., Siotto, M., Lott, C., Innocenti, F.Degli, 2012. Laboratory test methods to determine the degradation of plastics in marine environmental conditions. Front Microbiol 3, 225.
[7] Shen, M., Zhang, Y., Zhu, Y., Song, B., Zeng, G., Hu, D., Wen, X., Ren, X., 2019. Recent advances in toxicological research of nanoplastics in the environment: a review. Environ Pollut 252 (Pt A), 511–521.
[8] Wang, L., Wu, W.M., Bolan, N.S., Tsang, D.C.W., Li, Y., Qin, M., Hou, D., 2021. Environmental fate, toxicity and risk management strategies of nanoplastics in the environment: current status and future perspectives. J Hazard Mater 401, 123415.
[9] De Felice, B., Sugni, M., Casati, L., Parolini, M., 2022. Molecular, biochemical and behavioral responses of Daphnia magna under long-term exposure to polystyrene nanoplastics. Environ Int 164, 107264.
[10] Sugni, M., Balzano, A., De Felice, B., Bonasoro, F., Casati, L., Madaschi, L., Ascagni, M., Parolini, M., 2024. Exposure to polystyrene nanoplastics induced physiological and behavioral effects on the brittle star Ophiactis virens. Mar Pollut Bull 200, 116061.
[11] Masseroni, A., Ribeiro, M., Becchi, A., Saliu, F., Granadeiro, C.M., Villa, S., Urani, C., Santos, M.M., 2025. Effects of nano- and micro- fibers derived from surgical face masks in Danio rerio. Aquat Toxicol 283, 107349.
[12] Wang, Y., Nan, X., Sun, H., Shi, Y., Miao, J., Li, Y., Han, X., Zhang, N., Wang, H., Ren, N., Zhao, X., Liu, B., 2024. From insects to mammals! Tissue accumulation and transgenerational transfer of micro/nano-plastics through the food chain. J Hazard Mater 480, 136424.
[13] Sangkham, S., Faikhaw, O., Munkong, N., Sakunkoo, P., Arunlertaree, C., Chavali, M., Mousazadeh, M., Tiwari, A., 2022. A review on microplastics and nanoplastics in the environment: Their occurrence, exposure routes, toxic studies, and potential effects on human health. Mar Pollut Bull 181, 113832.
[14] Leslie, H.A., van Velzen, M.J.M., Brandsma, S.H., Vethaak, A.D., Garcia-Vallejo, J. J., Lamoree, M.H., 2022. Discovery and quantification of plastic particle pollution in human blood. Environ Int 163, 107199.
[15] Yee, M.S., Hii, L.W., Looi, C.K., Lim, W.M., Wong, S.F., Kok, Y.Y., Tan, B.K., Wong, C.Y., Leong, C.O., 2021. Impact of Microplastics and Nanoplastics on Human Health. Nanomaterials 11 (2).
[16] Nihart, A.J., Garcia, M.A., El Hayek, E., Liu, R., Olewine, M., Kingston, J.D., Castillo, E.F., Gullapalli, R.R., Howard, T., Bleske, B., Scott, J., Gonzalez-Estrella, J., Gross, J.M., Spilde, M., Adolphi, N.L., Gallego, D.F., Jarrell, H.S., Dvorscak, G., Zuluaga-Ruiz, M.E., West, A.B., Campen, M.J., 2025. Bioaccumulation of microplastics in decedent human brains. Nat Med.
[17] de Sousa, A.K.A., Pires, K.S.N., Cavalcante, I.H., Cavalcante, I.C.L., Santos, J.D., Queiroz, M.I.C., Leite, A.C.R., Crispim, A.C., da Rocha, E.R., 2024. Junior, T.M. Aquino, R.B. Weingrill, J. Urschitz, S. Ospina-Prieto, A.U. Borbely, Polystyrene microplastics exposition on human placental explants induces time-dependent cytotoxicity, oxidative stress and metabolic alterations. Front Endocrinol 15, 1481014.
[18] Bianchi, M.G., Casati, L., Sauro, G., Taurino, G., Griffini, E., Milani, C., Ventura, M., Bussolati, O., Chiu, M., 2025. Biological effects of micro-/nano-plastics in macrophages. Nanomaterials 15 (5).
[19] Marfella, R., Prattichizzo, F., Sardu, C., Fulgenzi, G., Graciotti, L., Spadoni, T., D'Onofrio, N., Scisciola, L., La Grotta, R., Frigé, C., Pellegrini, V., Municinò, M., Siniscalchi, M., Spinetti, F., Vigliotti, G., Vecchione, C., Carrizzo, A., Accarino, G., Squillante, A., Spaziano, G., Mirra, D., Esposito, R., Altieri, S., Falco, G., Fenti, A., Galoppo, S., Canzano, S., Sasso, F.C., Matacchione, G., Olivieri, F., Ferraraccio, F., Panarese, I., Paolisso, P., Barbato, E., Lubritto, C., Balestrieri, M.L., Mauro, C., Caballero, A.E., Rajagopalan, S., Ceriello, A., D'Agostino, B., Iovino, P., Paolisso, G., 2024. Microplastics and nanoplastics in atheromas and cardiovascular events. N Engl J Med 390 (10), 900–910.
[20] Guo, X., Wang, L., Wang, X., Li, D., Wang, H., Xu, H., Liu, Y., Kang, R., Chen, Q., Zheng, L., Wu, S., Guo, Z., Zhang, S., 2024. Discovery and analysis of microplastics in human bone marrow. J Hazard Mater 477, 135266.
[21] Jani, P., Halbert, G.W., Langridge, J., Florence, A.T., 1990. Nanoparticle uptake by the rat gastrointestinal mucosa: quantitation and particle size dependency. J Pharm Pharmacol 42 (12), 821–826.
[22] Jing, J., Zhang, L., Han, L., Wang, J., Zhang, W., Liu, Z., Gao, A., 2022. Polystyrene micro-/nanoplastics induced hematopoietic damages via the crosstalk of gut microbiota, metabolites, and cytokines. Environ Int 161, 107131.
[23] Giannandrea, D., Parolini, M., Citro, V., De Felice, B., Pezzotta, A., Abazari, N., Platonova, N., Sugni, M., Chiu, M., Villa, A., Lesma, E., Chiaramonte, R., Casati, L., 2024. Nanoplastic impact on bone microenvironment: a snapshot from murine bone cells. J Hazard Mater 462, 132717.
[24] Qiao, R., Sheng, C., Lu, Y., Zhang, Y., Ren, H., Lemos, B., 2019. Microplastics induce intestinal inflammation, oxidative stress, and disorders of metabolome and microbiome in zebrafish. Sci Total Environ 662, 246–253.
[25] Liu, Z., Yu, P., Cai, M., Wu, D., Zhang, M., Huang, Y., Zhao, Y., 2019. Polystyrene nanoplastic exposure induces immobilization, reproduction, and stress defense in the freshwater cladoceran Daphnia pulex. Chemosphere 215, 74–81.
[26] Parenti, C.C., Ghilardi, A., Della Torre, C., Magni, S., Del Giacco, L., Binelli, A., 2019. Evaluation of the infiltration of polystyrene nanobeads in zebrafish embryo tissues after short-term exposure and the related biochemical and behavioural effects. Environ Pollut 254 (Pt A), 112947.
[27] Lehner, R., Weder, C., Petri-Fink, A., Rothen-Rutishauser, B., 2019. Emergence of nanoplastic in the environment and possible impact on human health. Environ Sci Technol 53 (4), 1748–1765.
[28] Casati, L., Pagani, F., Limonta, P., Vanetti, C., Stancari, G., Sibilia, V., 2019. Beneficial effects of delta-tocotrienol against oxidative stress in osteoblastic cells: studies on the mechanisms of action. Eur J Nutr.
[29] Sibilia, V., Bottai, D., Maggi, R., Pagani, F., Chiaramonte, R., Giannandrea, D., Citro, V., Platonova, N., Casati, L., 2021. Sex steroid regulation of oxidative stress in bone cells: an in vitro study. Int J Environ Res Public Health 18 (22).
[30] Croucher, P.I., McDonald, M.M., Martin, T.J., 2016. Bone metastasis: the importance of the neighbourhood. Nat Rev Cancer 16 (6), 373–386.
[31] Chiu, M., Toscani, D., Marchica, V., Taurino, G., Costa, F., Bianchi, M.G., Andreoli, R., Franceschi, V., Storti, P., Burroughs-Garcia, J., Eufemiese, R.A., Dalla Palma, B., Campanini, N., Martella, E., Mancini, C., Shan, J., Kilberg, M.S., D'Amico, G., Dander, E., Agnelli, L., Pruneri, G., Donofrio, G., Bussolati, O., Giuliani, N., 2020. Myeloma cells deplete bone marrow glutamine and inhibit osteoblast differentiation limiting asparagine availability. Cancers 12 (11).
[32] Capp, J.P., Bataille, R., 2022. A bone paradigm challenging the standard model of myeloma oncogenesis. Crit Rev Oncol Hematol 172, 103640.
[33] Wan, X., Zhang, W., Dai, L., Chen, L., 2024. The role of extracellular vesicles in bone regeneration and associated bone diseases. Curr Issues Mol Biol 46 (9), 9269–9285.
[34] van Niel, G., D'Angelo, G., Raposo, G., 2018. Shedding light on the cell biology of extracellular vesicles. Nat Rev Mol Cell Biol 19 (4), 213–228.
[35] Lay, S.Le, Rome, S., Loyer, X., Nieto, L., 2021. Adipocyte-derived extracellular vesicles in health and diseases: nano-packages with vast biological properties. FASEB Bioadv 3 (6), 407–419.
[36] Zhang, L., Lei, Q., Wang, H., Xu, C., Liu, T., Kong, F., Yang, C., Yan, G., Sun, L., Zhao, A., Chen, W., Hu, Y., Xie, H., Cao, Y., Fu, F., Yuan, G., Chen, Z., Guo, A.Y., Li, Q., 2019. Tumor-derived extracellular vesicles inhibit osteogenesis and exacerbate myeloma bone disease. Theranostics 9 (1), 196–209.
[37] Cloos, A.S., Ghodsi, M., Stommen, A., Vanderroost, J., Dauguet, N., Pollet, H., Auria, L.D., Mignolet, E., Larondelle, Y., Terrasi, R., Muccioli, G.G., Van Der Smissen, P., Tyteca, D., 2020. Interplay between plasma membrane lipid alteration, oxidative stress and calcium-based mechanism for extracellular vesicle biogenesis from erythrocytes during blood storage. Front Physiol 11, 712.
[38] Sa, J., Lv, Y., He, J., Wang, K., Zhou, J., 2026. Bidirectional interactions between nanomaterials and extracellular vesicles: molecular insights and translational implications. Int J Nanomed 21, 585732.
[39] Calzoni, E., Montegiove, N., Cesaretti, A., Bertoldi, A., Cusumano, G., Gigliotti, G., Emiliani, C., 2024. Microplastic and extracellular vesicle interactions: recent studies on human health and environment risks. Biophysica 4 (4), 724–746.
[40] Lima, T.S.M., Souza, W., Geaquinto, L.R.O., Sanches, P.L., Stepień, E.L., Meneses, J., Fernández-de Gortari, E., Meisner-Kober, N., Himly, M., Granjeiro, J. M., Ribeiro, A.R., 2022. Nanomaterial exposure, extracellular vesicle biogenesis and adverse cellular outcomes: a scoping review. Nanomaterials 12 (7).
[41] Wang, C., Stöckl, S., Li, S., Herrmann, M., Lukas, C., Reinders, Y., Sickmann, A., Grässel, S., 2022. Effects of extracellular vesicles from osteogenic differentiated human BMSCs on osteogenic and adipogenic differentiation capacity of naïve human BMSCs. Cells 11 (16).
[42] Giannandrea, D., Platonova, N., Colombo, M., Mazzola, M., Citro, V., Adami, R., Maltoni, F., Ancona, S., Dolo, V., Giusti, I., Basile, A., Pistocchi, A., Cantone, L., Bollati, V., Casati, L., Calzavara, E., Turrini, M., Lesma, E., Chiaramonte, R., 2022. Extracellular vesicles mediate the communication between multiple myeloma and bone marrow microenvironment in a NOTCH dependent way. Haematologica 107 (9), 2183–2194.
[43] Faict, S., Muller, J., De Veirman, K., De Bruyne, E., Maes, K., Vrancken, L., Heusschen, R., De Raeve, H., Schots, R., Vanderkerken, K., Caers, J., Menu, E.,

2018. Exosomes play a role in multiple myeloma bone disease and tumor development by targeting osteoclasts and osteoblasts. Blood Cancer J 8 (11), 105.
[44] Mrak, E., Casati, L., Pagani, F., Rubinacci, A., Zarattini, G., Sibilia, V., 2015. Ghrelin increases beta-catenin level through protein kinase A activation and regulates OPG expression in rat primary osteoblasts. Int J Endocrinol 2015, 547473.
[45] Casati, L., Pagani, F., Maggi, R., Ferrucci, F., Sibilia, V., 2020. Food for bone: evidence for a role for delta-tocotrienol in the physiological control of osteoblast migration. Int J Mol Sci 21 (13).
[46] Villa, A., Garofalo, M., Crescenti, D., Rizzi, N., Brunialti, E., Vingiani, A., Belotti, P., Sposito, C., Franzè, S., Cilurzo, F., Pruneri, G., Recordati, C., Giudice, C., Giordano, A., Tortoreto, M., Beretta, G., Stefanello, D., Manenti, G., Zaffaroni, N., Mazzaferro, V., Ciana, P., 2021. Transplantation of autologous extracellular vesicles for cancer-specific targeting. Theranostics 11 (5), 2034–2047.
[47] Casati, L., Pagani, F., Braga, P.C., Lo Scalzo, R., Sibilia, V., 2016. Nasunin, a new player in the field of osteoblast protection against oxidative stress. J Funct Foods 23, 474–484.
[48] Casati, L., Pagani, F., Fibiani, M., Lo Scalzo, R., Sibilia, V., 2019. Potential of delphinidin-3-rutinoside extracted from Solanum melongena L. as promoter of osteoblastic MC3T3-E1 function and antagonist of oxidative damage. Eur J Nutr 58 (3), 1019–1032.
[49] Plakhova, N., Panagopoulos, V., Cantley, M.D., Trainor, L.J., Hewett, D.R., Clark, K.C., Gardiner, J., Yong, A., Lee, C., Horvath, N., Croucher, P.I., Cakouros, D., Stewart, S.A., Gronthos, S., Zannettino, A.C.W., Mrozik, K.M., Vandyke, K., 2025. Age-related mesenchymal stromal cell senescence is associated with progression from MGUS to multiple myeloma. Leukemia 39 (6), 1464–1475.
[50] de Paula, F.J.A., Rosen, C.J., 2020. Marrow adipocytes: origin, structure, and function. Annu Rev Physiol 82, 461–484.
[51] Shurtleff, M.J., Temoche-Diaz, M.M., Karfilis, K.V., Ri, S., Schekman, R., 2016. Y-box protein 1 is required to sort microRNAs into exosomes in cells and in a cell-free reaction. Elife 5.
[52] Villarroya-Beltri, C., Gutiérrez-Vázquez, C., Sánchez-Cabo, F., Pérez-Hernández, D., Vázquez, J., Martin-Cofreces, N., Martinez-Herrera, D.J., Pascual-Montano, A., Mittelbrunn, M., Sánchez-Madrid, F., 2013. Sumoylated hnRNPA2B1 controls the sorting of miRNAs into exosomes through binding to specific motifs. Nat Commun 4, 2980.
[53] Santangelo, L., Giurato, G., Cicchini, C., Montaldo, C., Mancone, C., Tarallo, R., Battistelli, C., Alonzi, T., Weisz, A., Tripodi, M., 2016. The RNA-binding protein SYNCRIP is a component of the hepatocyte exosomal machinery controlling MicroRNA sorting. Cell Rep 17 (3), 799–808.
[54] Mazziotta, C., Lanzillotti, C., Iaquinta, M.R., Taraballi, F., Torreggiani, E., Rotondo, J.C., Otòn-Gonzalez, L., Mazzoni, E., Frontini, F., Bononi, I., De Mattei, M., Tognon, M., Martini, F., 2021. MicroRNAs modulate signaling pathways in osteogenic differentiation of mesenchymal stem cells. Int J Mol Sci 22 (5).
[55] Zhang, C., Xu, X., Trotter, T.N., Gowda, P.S., Lu, Y., Suto, M.J., Javed, A., Murphy-Ullrich, J.E., Li, J., Yang, Y., 2022. Runx2 Deficiency in Osteoblasts Promotes Myeloma Resistance to Bortezomib by Increasing TSP-1-Dependent TGFβ1 Activation and Suppressing Immunity in Bone Marrow. Mol Cancer Ther 21 (2), 347–358.
[56] Yang, Q., Peng, Y., Wu, X., Cao, X., Zhang, P., Liang, Z., Zhang, J., Zhang, Y., Gao, P., Fu, Y., Liu, P., Cao, Z., Ding, T., 2025. Microplastics in human skeletal tissues: presence, distribution and health implications. Environ Int 196, 109316.
[57] Han, J., Yang, K., An, J., Jiang, N., Fu, S., Tang, X., 2022. The role of NRF2 in bone metabolism - friend or foe? Front Endocrinol 13, 813057.
[58] Mierzejewski, K., Kurzyńska, A., Golubska, M., Gałęcka, I., Całka, J., Bogacka, I., 2025. Extracellular vesicles as mediators of metabolomic changes in response to PET microplastics. Environ Pollut 385, 127047.
[59] Hoshino, A., Costa-Silva, B., Shen, T.L., Rodrigues, G., Hashimoto, A., Tesic Mark, M., Molina, H., Kohsaka, S., Di Giannatale, A., Ceder, S., Singh, S., Williams, C., Soplop, N., Uryu, K., Pharmer, L., King, T., Bojmar, L., Davies, A.E., Ararso, Y., Zhang, T., Zhang, H., Hernandez, J., Weiss, J.M., Dumont-Cole, V.D., Kramer, K., Wexler, L.H., Narendran, A., Schwartz, G.K., Healey, J.H., Sandstrom, P., Labori, K.J., Kure, E.H., Grandgenett, P.M., Hollingsworth, M.A., de Sousa, M., Kaur, S., Jain, M., Mallya, K., Batra, S.K., Jarnagin, W.R., Brady, M.S., Fodstad, O., Muller, V., Pantel, K., Minn, A.J., Bissell, M.J., Garcia, B.A., Kang, Y., Rajasekhar, V.K., Ghajar, C.M., Matei, I., Peinado, H., Bromberg, J., Lyden, D., 2015. Tumour exosome integrins determine organotropic metastasis. Nature 527 (7578), 329–335.
[60] Park, M.N., Kim, M., Lee, S., Kang, S., Ahn, C.H., Tallei, T.E., Kim, W., Kim, B., 2025. Targeting redox signaling through exosomal MicroRNA: insights into tumor microenvironment and precision oncology. Antioxidants 14 (5).
[61] Bhavsar, V., Sahu, A., Taware, R., 2024. Stress-induced extracellular vesicles: insight into their altered proteomic composition and probable physiological role in cancer. Mol Cell Biochem.
[62] Loboda, A., Damulewicz, M., Pyza, E., Jozkowicz, A., Dulak, J., 2016. Role of Nrf2/HO-1 system in development, oxidative stress response and diseases: an evolutionarily conserved mechanism. Cell Mol Life Sci 73 (17), 3221–3247.
[63] Tang, Y., Zhou, Y., Fan, S., Wen, Q., 2022. The multiple roles and therapeutic potential of HSP60 in cancer. Biochem Pharmacol 201, 115096.
[64] Welsh, J.A., Goberdhan, D.C.I., O'Driscoll, L., Buzas, E.I., Blenkiron, C., Bussolati, B., Cai, H., Di Vizio, D., Driedonks, T.A.P., Erdbrügger, U., Falcon-Perez, J.M., Fu, Q.L., Hill, A.F., Lenassi, M., Lim, S.K., Mahoney, M.G., Mohanty, S., Möller, A., Nieuwland, R., Ochiya, T., Sahoo, S., Torrecilhas, A.C., Zheng, L., Zijlstra, A., Abuelreich, S., Bagabas, R., Bergese, P., Bridges, E.M., Brucale, M., Burger, D., Carney, R.P., Cocucci, E., Crescitelli, R., Hanser, E., Harris, A.L., Haughey, N.J., Hendrix, A., Ivanov, A.R., Jovanovic-Talisman, T., Kruh-Garcia, N. A., Ku'ulei-Lyn Faustino, V., Kyburz, D., Lässer, C., Lennon, K.M., Lötvall, J., Maddox, A.L., Martens-Uzunova, E.S., Mizenko, R.R., Newman, L.A., Ridolfi, A., Rohde, E., Rojalin, T., Rowland, A., Saftics, A., Sandau, U.S., Saugstad, J.A., Shekari, F., Swift, S., Ter-Ovanesyan, D., Tosar, J.P., Useckaite, Z., Valle, F., Varga, Z., van der Pol, E., van Herwijnen, M.J.C., Wauben, M.H.M., Wehman, A.M., Williams, S., Zendrini, A., Zimmerman, A.J., Théry, C., Witwer, K.W., Consortium, M., 2024. Minimal information for studies of extracellular vesicles (MISEV2023): from basic to advanced approaches. J Extracell Vesicles 13 (2), e12404.
[65] Mao, Y., Li, H., Huangfu, X., Liu, Y., He, Q., 2020. Nanoplastics display strong stability in aqueous environments: Insights from aggregation behaviour and theoretical calculations. Environ Pollut 258, 113760.
[66] Pelepenko, L.E., de Oliveira, M.C., Masaro, D.A., Lustosa, G.M.M.M., Mazon, T., Castilho, R.F., Dos Reis, L.M., Mac-Way, F., Hénaut, L., Kamel, S., Louvet, L., Oliveira, R.B., 2025. Effects of microplastics on the bones: a comprehensive review. Osteoporos Int 36 (8), 1327–1345.
[67] Broad, K., Walker, S.A., Davidovich, I., Witwer, K., Talmon, Y., Wolfram, J., 2023. Unraveling multilayered extracellular vesicles: speculation on cause. J Extracell Vesicles 12 (2), e12309.
[68] Kopac, T., 2021. Protein corona, understanding the nanoparticle-protein interactions and future perspectives: a critical review. Int J Biol Macromol 169, 290–301.
[69] Yu, Y., Luan, Y., Dai, W., 2022. Time evolution of protein corona formed by polystyrene nanoplastics and urease. Int J Biol Macromol 218, 72–81.
[70] Wu, D., Ma, Y., Cao, Y., Zhang, T., 2020. Mitochondrial toxicity of nanomaterials. Sci Total Environ 702, 134994.
[71] Dong, P.X., Song, X., Wu, J., Cui, S., Wang, G., Zhang, L., Sun, H., 2020. The fate of SWCNTs in mouse peritoneal macrophages: exocytosis, biodegradation, and sustainable retention. Front Bioeng Biotechnol 8, 211.
[72] Dumontel, B., Susa, F., Limongi, T., Canta, M., Racca, L., Chiodoni, A., Garino, N., Chiabotto, G., Centomo, M.L., Pignochino, Y., Cauda, V., 2019. ZnO nanocrystals shuttled by extracellular vesicles as effective Trojan nano-horses against cancer cells. Nanomed 14 (21), 2815–2833.
[73] Hao, F., Ku, T., Yang, X., Liu, Q.S., Zhao, X., Faiola, F., Zhou, Q., Jiang, G., 2020. Gold nanoparticles change small extracellular vesicle attributes of mouse embryonic stem cells. Nanoscale 12 (29), 15631–15637.
[74] Whiteside, T.L., 2018. Exosome and mesenchymal stem cell cross-talk in the tumor microenvironment. Semin Immunol 35, 69–79.